

We thank Dr S. Mitsuhashi for technical assistance in native blue PAGE and Dr M. C. V. Malicdan for editing the manuscript.

Potential Conflicts of Interest

I. Nishino: grants/grants pending, Ministry of Education, Culture, Sports, Science, and Technology (Japan); Ministry of Health, Labor, and Welfare (Japan); Neuromuscular Foundation (USA); Japan Foundation for Neuroscience and Mental Health (indirectly from Genzyme); patents pending or planned, method to develop model mouse for distal myopathy with rimmed vacuoles/hereditary inclusion body myopathy; development of therapy for distal myopathy with rimmed vacuoles/hereditary inclusion body myopathy; method to diagnose congenital muscular dystrophy with mitochondrial structural abnormalities; travel expenses, Neuromuscular Foundation.

References

- Emery AE. Emery-Dreifuss muscular dystrophy—a 40 year retrospective. *Neuromuscul Disord* 2000;10:228–232.
- Bione S, Maestrini E, Rivella S, et al. Identification of a novel X-linked gene responsible for Emery-Dreifuss muscular dystrophy. *Nat Genet* 1994;8:323–327.
- Bonne G, Di Barletta MR, Varnous S, et al. Mutations in the gene encoding lamin A/C cause autosomal dominant Emery-Dreifuss muscular dystrophy. *Nat Genet* 1999;21:285–288.
- Zhang Q, Bethmann C, Worth NF, et al. Nesprin-1 and -2 are involved in the pathogenesis of Emery Dreifuss muscular dystrophy and are critical for nuclear envelope integrity. *Hum Mol Genet* 2007;16:2816–2833.
- Gueneau L, Bertrand AT, Jais JP, et al. Mutations of the FHL1 gene cause Emery-Dreifuss muscular dystrophy. *Am J Hum Genet* 2009;85:338–353.
- Markiewicz E, Tilgner K, Barker N, et al. The inner nuclear membrane protein emerin regulates beta-catenin activity by restricting its accumulation in the nucleus. *EMBO J* 2006;25:3275–3285.
- Lammerding J, Hsiao J, Schulze PC, et al. Abnormal nuclear shape and impaired mechanotransduction in emerin-deficient cells. *J Cell Biol* 2005;170:781–791.
- Rowat AC, Lammerding J, Ipsen JH. Mechanical properties of the cell nucleus and the effect of emerin deficiency. *Biophys J* 2006;91:4649–4664.
- Holaska JM, Wilson KL. Multiple roles for emerin: implications for Emery-Dreifuss muscular dystrophy. *Anat Rec A Discov Mol Cell Evol Biol* 2006;288:676–680.
- Ura S, Hayashi YK, Goto K, et al. Limb-girdle muscular dystrophy due to emerin gene mutations. *Arch Neurol* 2007;64:1038–1041.
- Zhang X, Xu R, Zhu B, et al. Syne-1 and Syne-2 play crucial roles in myonuclear anchorage and motor neuron innervation. *Development* 2007;134:901–908.
- Kandert S, Luke Y, Kleinhenz T, et al. Nesprin-2 giant safeguards nuclear envelope architecture in LMNA S143F progeria cells. *Hum Mol Genet* 2007;16:2944–2959.
- Holaska JM, Wilson KL, Mansharamani M. The nuclear envelope, lamins and nuclear assembly. *Curr Opin Cell Biol* 2002;14:357–364.
- Broers JL, Kuijpers HJ, Ostlund C, et al. Both lamin A and lamin C mutations cause lamina instability as well as loss of internal nuclear lamin organization. *Exp Cell Res* 2005;304:582–592.
- Lee JS, Hale CM, Panorchan P, et al. Nuclear lamin A/C deficiency induces defects in cell mechanics, polarization, and migration. *Biophys J* 2007;93:2542–2552.
- Crisp M, Liu Q, Roux K, et al. Coupling of the nucleus and cytoplasm: role of the LINC complex. *J Cell Biol* 2006;172:41–53.
- Capell BC, Collins FS. Human laminopathies: nuclei gone genetically awry. *Nat Rev Genet* 2006;7:940–952.
- Bonne G, Yaou RB, Beroud C, et al. 108th ENMC International Workshop, 3rd Workshop of the MYO-CLUSTER project: EURO-MEN, 7th International Emery-Dreifuss Muscular Dystrophy (EDMD) Workshop, 13-15 September 2002, Naarden, the Netherlands. *Neuromuscul Disord* 2003;13:508–515.
- Dreger M, Bengtsson L, Schoneberg T, et al. Nuclear envelope proteomics: novel integral membrane proteins of the inner nuclear membrane. *Proc Natl Acad Sci U S A* 2001;98:11943–11948.
- Merner ND, Hodgkinson KA, Haywood AF, et al. Arrhythmogenic right ventricular cardiomyopathy type 5 is a fully penetrant, lethal arrhythmic disorder caused by a missense mutation in the *TMEM43* gene. *Am J Hum Genet* 2008;82:809–821.
- Bengtsson L, Otto H. LUMA interacts with emerin and influences its distribution at the inner nuclear membrane. *J Cell Sci* 2008;121:536–548.
- Holaska JM, Wilson KL. An emerin “proteome”: purification of distinct emerin-containing complexes from HeLa cells suggests molecular basis for diverse roles including gene regulation, mRNA splicing, signaling, mechanosensing, and nuclear architecture. *Biochemistry* 2007;46:8897–8908.
- Fink AL. Natively unfolded proteins. *Curr Opin Struct Biol* 2005;15:35–41.
- Ostlund C, Ellenberg J, Hallberg E, et al. Intracellular trafficking of emerin, the Emery-Dreifuss muscular dystrophy protein. *J Cell Sci* 1999;112(pt 11):1709–1719.
- Salina D, Bodoor K, Enarson P, et al. Nuclear envelope dynamics. *Biochem Cell Biol* 2001;79:533–542.
- Zuleger N, Korfali N, Schirmer EC. Inner nuclear membrane protein transport is mediated by multiple mechanisms. *Biochem Soc Trans* 2008;36:1373–1377.
- Sullivan T, Escalante-Alcalde D, Bhatt H, et al. Loss of A-type lamin expression compromises nuclear envelope integrity leading to muscular dystrophy. *J Cell Biol* 1999;147:913–920.
- Haque F, Lloyd DJ, Smallwood DT, et al. SUN1 interacts with nuclear lamin A and cytoplasmic nesprins to provide a physical connection between the nuclear lamina and the cytoskeleton. *Mol Cell Biol* 2006;26:3738–3751.
- Stewart-Hutchinson PJ, Hale CM, Wirtz D, Hodzic D. Structural requirements for the assembly of LINC complexes and their function in cellular mechanical stiffness. *Exp Cell Res* 2008;314:1892–1905.
- Lei K, Zhang X, Ding X, et al. SUN1 and SUN2 play critical but partially redundant roles in anchoring nuclei in skeletal muscle cells in mice. *Proc Natl Acad Sci U S A* 2009;106:10207–10212.
- Puckelwartz MJ, Kessler E, Zhang Y, et al. Disruption of nesprin-1 produces an Emery Dreifuss muscular dystrophy-like phenotype in mice. *Hum Mol Genet* 2009;18:607–620.
- Haque F, Mazzeo D, Patel JT, et al. Mammalian SUN protein networks at the inner nuclear membrane and their role in laminopathy disease processes. *J Biol Chem* 2010;285:3487–3498.
- Raharjo WH, Enarson P, Sullivan T, et al. Nuclear envelope defects associated with LMNA mutations cause dilated cardiomyopathy and Emery-Dreifuss muscular dystrophy. *J Cell Sci* 2001;114:4447–4457.
- Razafsky D, Hodzic D. Bringing KASH under the SUN: the many faces of nucleo-cytoskeletal connections. *J Cell Biol* 2009;186:461–472.

A Congenital Muscular Dystrophy with Mitochondrial Structural Abnormalities Caused by Defective De Novo Phosphatidylcholine Biosynthesis

Satomi Mitsuhashi,¹ Aya Ohkuma,¹ Beril Talim,² Minako Karahashi,³ Tomoko Koumura,³ Chieko Aoyama,⁴ Mana Kurihara,⁵ Ros Quinlivan,^{6,7} Caroline Sewry,^{6,8} Hiroaki Mitsuhashi,¹ Kanako Goto,¹ Burcu Koksal,² Gulsev Kale,² Kazutaka Ikeda,⁹ Ryo Taguchi,⁹ Satoru Noguchi,¹ Yukiko K. Hayashi,¹ Ikuya Nonaka,¹ Roger B. Sher,¹⁰ Hiroyuki Sugimoto,⁴ Yasuhito Nakagawa,³ Gregory A. Cox,¹⁰ Haluk Topaloglu,¹¹ and Ichizo Nishino^{1,*}

Congenital muscular dystrophy is a heterogeneous group of inherited muscle diseases characterized clinically by muscle weakness and hypotonia in early infancy. A number of genes harboring causative mutations have been identified, but several cases of congenital muscular dystrophy remain molecularly unresolved. We examined 15 individuals with a congenital muscular dystrophy characterized by early-onset muscle wasting, mental retardation, and peculiar enlarged mitochondria that are prevalent toward the periphery of the fibers but are sparse in the center on muscle biopsy, and we have identified homozygous or compound heterozygous mutations in the gene encoding choline kinase beta (*CHKB*). This is the first enzymatic step in a biosynthetic pathway for phosphatidylcholine, the most abundant phospholipid in eukaryotes. In muscle of three affected individuals with nonsense mutations, choline kinase activities were undetectable, and phosphatidylcholine levels were decreased. We identified the human disease caused by disruption of a phospholipid de novo biosynthetic pathway, demonstrating the pivotal role of phosphatidylcholine in muscle and brain.

A spontaneous mutant mouse with a neonatal-onset autosomal-recessive rostral-to-caudal muscular dystrophy (*rmd* mouse) due to a loss-of-function mutation in choline kinase beta (*Chkb*) was identified in 2006.¹ Interestingly, *rmd* mice exhibit a unique mitochondrial morphology in muscle fibers, which show enlarged mitochondria at the periphery of the fiber but none at the center (Figure S1). These features are similar to those seen in a congenital muscular dystrophy (CMD) that we previously reported in four Japanese individuals.² We therefore screened 15 genetically undiagnosed cases of CMD with fairly homogeneous clinical features (Table 1) for mutations in choline kinase beta (*CHKB*); we included the four cases from in our previous study in these 15 cases. Features included peculiar mitochondrial changes in muscle as well as motor delay followed by the appearance of severe mental retardation and microcephaly without structural brain abnormalities (Figure 1 and Table 1).

All clinical materials used in this study were obtained for diagnostic purposes with written informed consent. The study was approved by the Ethical Committee of the National Center of Neurology and Psychiatry. All mouse protocols were approved by the Ethical Review Committee on the Care and Use of Rodents in the National Institute of Neuroscience, National Center of Neurology and Psychi-

atry. For muscle pathology, samples of skeletal muscle were obtained from biceps brachii or quadriceps femoris in humans and from quadriceps femoris muscle in 8-week-old *rmd* mice. Muscles were frozen and sectioned at a thickness of 10 μ m according to standard procedures, and a battery of routine histochemical stains, including hematoxylin and eosin (H&E), modified Gomori trichrome (mGT), NADH-tetrazolium reductase (NADH-TR), succinate dehydrogenase (SDH), cytochrome c oxidase (COX), and Oil Red O, were analyzed. For electron microscopic analysis, muscles were fixed as previously described,³ and ultra-thin sections were observed at 120kV or 80kV. All affected individuals exhibited nonspecific dystrophic features (Figure 1A). However, in mGT, NADH-TR, SDH, and COX staining, prominent mitochondria at the periphery as well as central areas devoid of mitochondria were seen (Figures 1B and 1C). Oil Red O staining was unremarkable (data not shown). Electron microscopy confirmed enlarged mitochondria (Figure 1D).

We directly sequenced all exons and their flanking intronic regions in *CHKB* (MIM 612395, NM_005198.4, GenBank Gene ID 1120) in genomic DNA extracted from individuals' peripheral lymphocytes. All 15 individuals in three different populations (Japanese, Turkish, and British) had homozygous or compound heterozygous mutations in

¹National Institute of Neuroscience, Department of Neuromuscular Research, National Center of Neurology and Psychiatry, Tokyo 1878502, Japan; ²Department of Pediatrics, Pathology Unit, Hacettepe Children's Hospital, Ankara, 06100, Turkey; ³School of Pharmaceutical Sciences, Kitasato University, Tokyo, 108864, Japan; ⁴Department of Biochemistry, Dokkyo Medical University School of Medicine, Mibu, 3210293, Japan; ⁵Department of Pediatrics, The Kanagawa Rehabilitation Center, Kanagawa, 2430121, Japan; ⁶Dubowitz Neuromuscular Centre, Great Ormond Street Hospital for Children NHS Trust, London, WC1N 3JH, UK; ⁷MRC Centre for Neuromuscular Disorders, National Hospital for Neurology and Neurosurgery, Queen Square, London, WC1N 3BG, UK; ⁸RJAH Orthopaedic Hospital, Oswestry, SY107AG, UK; ⁹Department of Metabolome, Graduate School of Medicine, The University of Tokyo, Tokyo, 113003, Japan; ¹⁰The Jackson Laboratory, Bar Harbor, Maine, 04609, USA; ¹¹Department of Pediatrics, Child Neurology Unit, Hacettepe Children's Hospital, 06100, Ankara, Turkey

*Correspondence: nishino@ncnp.go.jp

DOI 10.1016/j.ajhg.2011.05.010. ©2011 by The American Society of Human Genetics. All rights reserved.

Table 1. Summary of Clinical and Laboratory Features

Individual	Sex	Origin	Phenotypic Findings							Muscle Pathology					Mutations				Literature ref. on phenotype		
			Age at Last Follow-Up	Floppy at Birth	Walk Alone	Serum Creatine Kinase (IU/liter)	Head Circumference (percentile)	Mental Retardation	Seizure	Cardiomyopathy	Skin Change	Age at Muscle Biopsy	Necrotic Fiber	Regenerative Fiber	Endomyxial Fibrosis	Mitochondrial Enlargement	Status	cDNA		Consequence	Exon
1	F	Japanese	died at 13 yr	+	2 yr 6 mo	370	ND	+	-	+	-	7 yr 3 mo	+	+	+	+	homo	c.810T>A	p.Tyr270X	7	2
2	M	Japanese	died at 23 yr	+	1 yr 9 mo	190–2676	25–50	+	+	+	-	1 yr 2 mo	+	+	+	+	homo	c.810T>A	p.Tyr270X	7	2
3	F	Japanese	28 yr	+	1 yr 6 mo	502	ND	+	+	+	-	8 yr	+	+	+	+	het	c.116C>A	p.Ser39X	1	2
4	M	Japanese	22 yr	+	2 yr 6 mo	230	3–10	+	+	-	-	4 yr 11 mo	+	+	+	+	het	c.458dup	p.Leu153PhefsX57	3	2
																	het	c.116C>A	p.Ser39X	1	
4	M	Japanese	22 yr	+	2 yr 6 mo	230	3–10	+	+	-	-	4 yr 11 mo	+	+	+	+	het	c.458dup	p.Leu153PhefsX57	3	
																	het	c.116C>A	p.Ser39X	1	
5	M	Turkish	7 yr	-	2 yr 6 mo	843	<3	+	-	-	+	6 yr	±	+	+	+	homo	c.611_612insC	p.Thr205AsnfsX5	5	
6 ^a	M	Turkish	died at 2 yr 6 mo	+	no	258	<3	+	-	+	-	1 yr 3 mo	±	±	+	+	homo	c.922C>T	p.Gln308X	8	
7	F	Turkish	2 yr	-	no	368	3–10	+	-	^b	-	9 mo	-	±	+	+	homo	c.847G>A	p.Glu283Lys	8	
8	M	Turkish	13 yr	ND	2 yr	1122	ND	+	-	-	-	12 yr 10 mo	±	±	+	+	homo	c.1130 G>T	p.Arg377Leu	11	
9	F	Turkish	17 yr	+	3 yr	2669	<3	+	-	ND	-	17 yr	±	±	+	+	homo	c.554_562del	p.Pro185_Trp187del	4	
10	F	Turkish	16 yr	+	3 yr	1103	<3	+	-	^c	+	3 yr	-	±	+	+	homo	c.677+1G>A	ND	5	
11	F	Turkish	3 yr 3 mo	+	no	497	10–25	+	-	ND	-	3 yr	±	-	+	+	homo	c.677+1G>A	ND	5	
12	F	Turkish	5 yr	-	3 yr 6 mo	467	25–50	+	-	^d	+	4 yr 6 mo	±	+	+	+	homo	c.677+1G>A	ND	5	
13	M	Turkish	3 yr 6 mo	+	no	428	<3	+	-	+	+	3 yr	+	+	+	+	homo	c.1031+1G>A	aberrant splicing	9	
14	F	Turkish	6 yr 4 mo	-	1 yr 3 mo	1606	3–10	+	-	+	-	4 yr	+	+	+	+	homo	c.1031+1G>A	ND	9	
15	M	British	died at 8 yr	-	3 yr 4 mo	607–1715	<3	+	-	+	+	2 yr 2 mo	+	-	+	+	homo	c.852_859del	p.Trp284X	8	

Detailed clinical information for individual 1 to 4 was previously described (2). Eleven CHKB mutations were identified in 15 affected individuals. All exhibited generalized muscle hypotonia and weakness from early infancy. Ambulation was delayed, and gait in those who achieved walking was limited. In addition, all displayed marked mental retardation, and most never acquired meaningful language. Microcephaly with head circumferences at or below the 3rd to 10th percentile was observed in most cases. Cranial magnetic resonance imaging showed no developmental brain defects. Six individuals had dilated cardiomyopathy, and two had cardiac anomaly. Individuals 1, 2, 6, and 15 died from cardiomyopathy at ages 13 yr, 23 yr, 2 yr 6 mo, and 8 yr, respectively. No one had respiratory insufficiency. Ichthyosiform skin changes were frequent. All showed mildly to moderately elevated serum creatine kinase (CK) levels. Individuals 7 and 9 also had homozygous single-nucleotide substitutions, c.902C>T (p.Thr301Ile) and c.983A>G (p.Gln328Arg), respectively. CHK activities of recombinant CHK-β proteins with p.Thr301Ile and p.Gln328Arg were only mildly decreased (Figure S2), suggesting these are likely to be neutral polymorphisms or only mildly hypomorphic mutations. Individuals 10, 11, and 12, who have same c.677+1G>A mutation, and individuals 13 and 14, who have same c.1031+1G>A mutation, are not siblings. Abbreviations are as follows: ND, not determined; p, percentile; F, female; and M, male.

^a An affected sibling had ichthyosis and died at age 6 years with cardiomyopathy.

^b Patent ductus arteriosus.

^c Atrial septal defect.

^d Mitral valve prolapse.

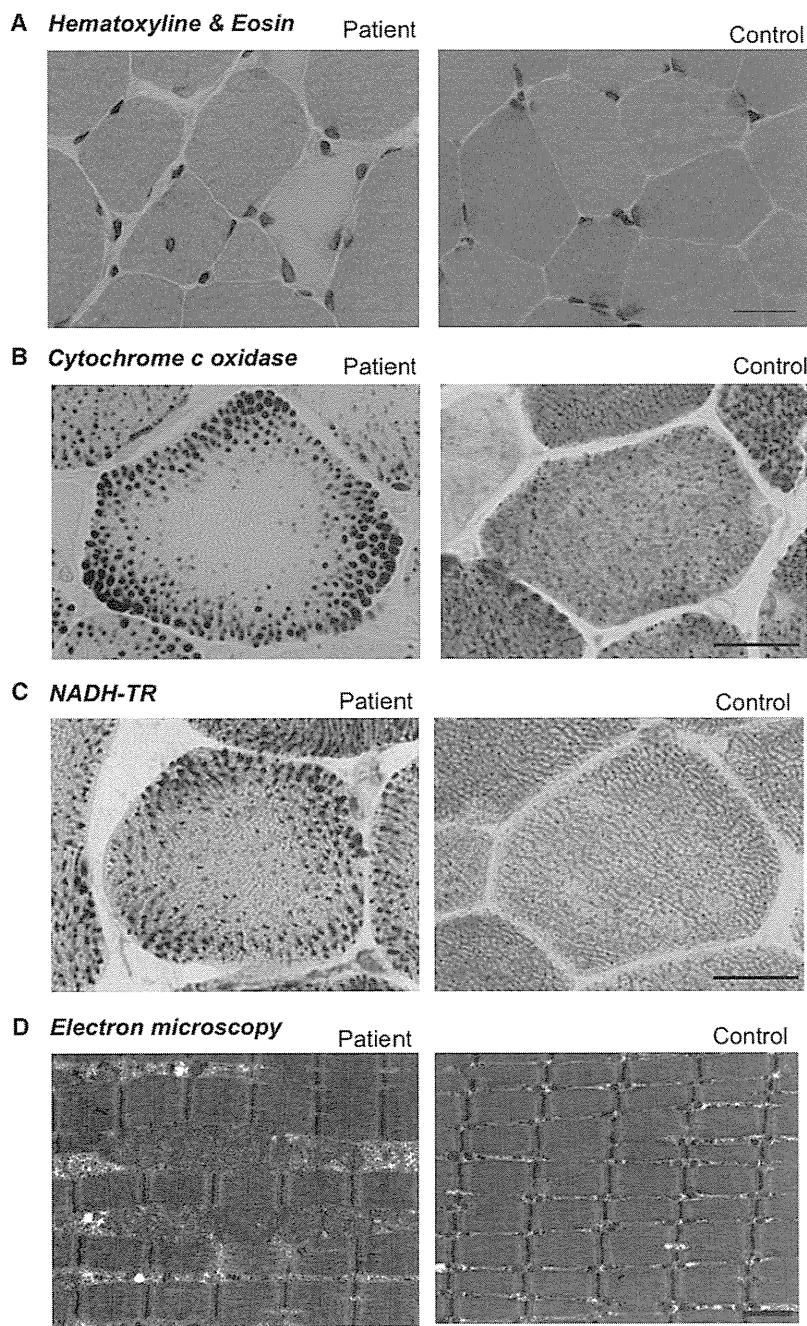


Figure 1. Muscle Pathology of the Affected Individuals

Cross-sections of muscle fiber from a human control and individual 4.

(A) On H&E staining, nonspecific dystrophic features with necrotic and regenerating fibers, internalized nuclei, and endomysial fibrosis are seen. The scale bar represents 25 μ m.

(B) On cytochrome c oxidase staining, enlarged mitochondria at the periphery and central areas devoid of mitochondria were seen. The scale bar represents 20 μ m.

(C) On NADH-TR staining, the intermyofibrillar network was preserved even in the central areas that are devoid of mitochondria, suggesting the presence of myofibrils and only absence of mitochondria. The scale bar represents 20 μ m.

(D) Electron microscopy confirmed enlarged mitochondria. The scale bar represents 1 μ m.

members of individual 1 and 2 were not available. Individuals 3 and 4 (siblings, Japanese) had the same compound heterozygous mutation c.116C>A (p.Ser39X) and c.458dup (p.Leu153PhefsX57). Both parents were healthy, and the father was heterozygous for mutation c.116C>A (p.Ser39X), whereas the mother was heterozygous for mutation c.458dup (p.Leu153-PhefsX57), thus confirming a recessive inheritance pattern. These mutations cosegregated with the disease phenotype in all family members tested.

We therefore measured CHK activity in biopsied muscle. For all biochemical analyses, because of the limiting amounts of remaining tissue, biopsied muscle samples were available only from individuals 2, 3, and 4. Biopsied muscle samples from these three individuals were homogenized in 3 volumes of 20 mM Tris-HCl (pH 7.5), 154 mM KCl, and 1 mM phenylmethanesulfonyl fluoride with a sonicator (MISONIX), and supernatant fractions (105,000 \times g, 60 min) were prepared and analyzed for CHK activity as

previously described.⁶ Similar to muscles of *rmd* mice,¹ muscles from individuals 2, 3, and 4, who carried homozygous or compound heterozygous nonsense mutations, did not have any detectable CHK activity (Figure 2A). Individuals 7, 8, and 9 had homozygous missense mutations c.847G>A (p.Glu283Lys) and c.1130 G>T (p.Arg377Leu) and a homozygous 3 amino acid deletion, c.554_562 del (p.Pro185_Trp187del), respectively. We screened 210 control chromosomes for the identified missense mutations and small in-frame deletion by direct sequencing or single-strand conformation polymorphism (SSCP) analysis. SSCP was performed with Gene Gel Excel (GE Healthcare) as previously described.⁷ These missense mutations and this small in-frame deletion were not identified in control

previously described.⁶ Similar to muscles of *rmd* mice,¹ muscles from individuals 2, 3, and 4, who carried homozygous or compound heterozygous nonsense mutations, did not have any detectable CHK activity (Figure 2A). Individuals 7, 8, and 9 had homozygous missense mutations c.847G>A (p.Glu283Lys) and c.1130 G>T (p.Arg377Leu) and a homozygous 3 amino acid deletion, c.554_562 del (p.Pro185_Trp187del), respectively. We screened 210 control chromosomes for the identified missense mutations and small in-frame deletion by direct sequencing or single-strand conformation polymorphism (SSCP) analysis. SSCP was performed with Gene Gel Excel (GE Healthcare) as previously described.⁷ These missense mutations and this small in-frame deletion were not identified in control

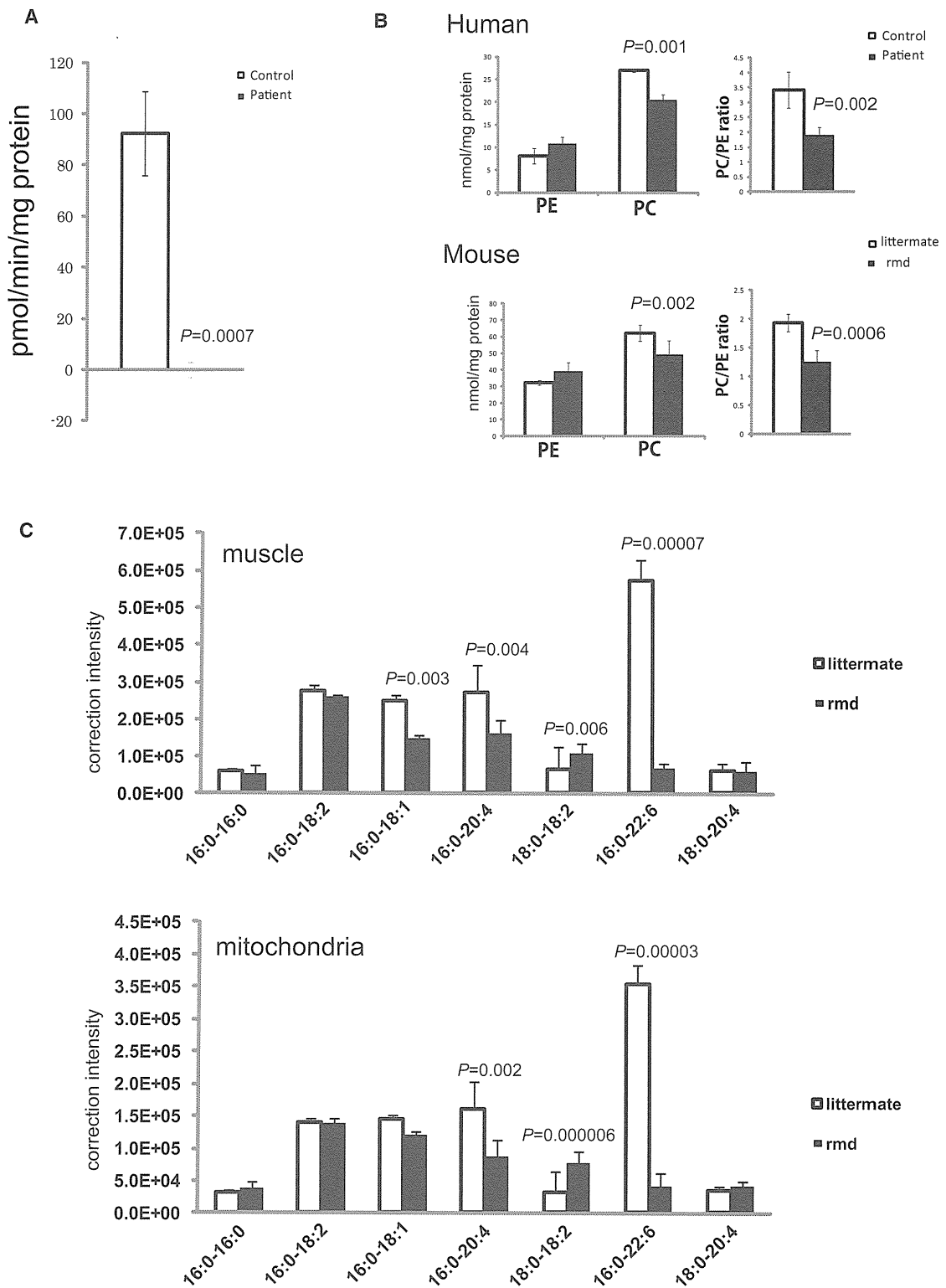


Figure 2. Choline Kinase Activity and Phospholipid Analyses

(A) In muscle tissue from individuals 2, 3, and 4, CHK activity cannot be detected ($n = 3$). Data represent the mean of three individuals. (B) PC and PE content in frozen biopsied muscle tissues from individuals 2, 3, and 4 and hindlimb muscles from 8-week-old *rmd* mice ($n = 4$) and control littermates ($n = 5$) were analyzed by thin-layer chromatography followed by phosphorus analysis. PC and the PC/PE ratio are significantly decreased in affected individuals and *rmd* mice ($n = 3$ for humans, $n = 4$ for *rmd* mice, $n = 5$ for littermates).

(C) Fatty acid composition of PC molecular species in muscles and isolated mitochondria from hindlimb muscles of *rmd* mice are determined by electrospray ionization mass spectrometry (ESI-MS). We observed that 34:1-PC (16:0-18:1), 36:4-PC (16:0-20:4), and 38:6-PC (16:0-22:6) species are significantly decreased, whereas 36:2-PC (18:0-18:2) is increased in *rmd* muscle. Similarly, in isolated mitochondria from hindlimb muscle, 36:4-PC (16:0-20:4) and 38:6-PC (16:0-22:6) species are decreased, whereas 36:2-PC (18:0-18:2) is increased.

chromosomes. To elucidate the pathogenesis of these substitutions, we measured CHK activity in recombinant proteins with mutations. We cloned the open reading frame of *CHKB* into pGEM-T easy (Promega), then subcloned it into pET15b (Novagen) to make His-tagged CHK- β .⁸ Each mutation was induced by site-directed mutagenesis.⁷ Plasmids were transformed into *Escherichia coli* strain BL21 (DE3) and inoculated at 20°C to an OD₆₀₀ of approximately 0.5, and the addition of 0.4 mM isopropyl- β -D-thiogalactopyranoside induced expression. The His-tagged CHK- β proteins were subjected to affinity purification on a nickel column (GE Healthcare) and eluted with 20 mM Tris-HCl (pH 7.4), 0.5 M NaCl, 300 mM imidazol, and 1 mM phenylmethanesulfonyl fluoride, and 25 ng protein was analyzed for CHK activity. CHK activity of recombinant proteins with these mutations decreased to less than 30% of wild-type CHK activity, suggesting that these mutations are causative in these individuals (Figure S2). For individual 13, who had a mutation at the splice site of the exon-intron border after exon 9 (c.1031+1G>A), we also analyzed cDNA sequences. Exons 4 through 10 were amplified from the first-strand cDNAs, and direct sequencing followed. cDNA analysis of *CHKB* in skeletal muscle from individual 13 showed four splicing variants, all of which remove consensus domains for *CHKB* (Figure S3). This suggests the same loss-of-function mechanism in humans and *rmd* mice.

Because phosphorylation of choline by CHK is the first enzymatic step for phosphatidylcholine (PC) biosynthesis,⁹ we anticipated that PC content should be altered in affected individuals' muscles. Phosphatidylcholine (PC), phosphatidylethanolamine (PE), and total phospholipid amounts were measured in biopsied muscles from individuals 2, 3, and 4 and in leg muscles from 8-week-old *rmd* mice by either one-dimensional or two-dimensional thin-layer chromatography (TLC) followed by phosphorus analysis.^{10,11} As expected, PC levels decreased in affected individuals' skeletal muscle (Figure 2B), as they did in *rmd* mice (Figure 2B and Sher et al.¹), suggesting that the CMDs due to *CHKB* mutations in humans and *rmd* mice are not only pathologically but also pathomechanistically similar.

PC is present in all tissues and accounts for around 50% of phospholipids in biological membranes in eukaryotes. Selective tissue involvement can be explained by the different tissue distribution of CHK isoforms. There are two CHK isoforms: CHK- α and CHK- β , encoded by distinct genes, *CHKA* (MIM 118491) and *CHKB*, respectively. They

are known to form both homodimers and heterodimers, with differential tissue distribution.¹² In mice, disruption of *Chka* causes embryonic lethality,¹³ suggesting the importance of CHK- α in embryonic development. In skeletal muscles from *rmd* mice, CHK activity is absent, and PC levels are decreased.¹ In other tissues, however, CHK activity is only mildly decreased, PC levels are not altered, and no obvious pathological change is seen.¹ CHK activity in skeletal muscle from individuals 2, 3, and 4 is barely detectable, and PC levels are significantly decreased, suggesting that CHK- β is the major isoform in human skeletal muscle. In support of this notion, CHK- α was not detected in human muscle (Figure S4). These results suggest that muscular dystrophy in affected individuals and *rmd* mice is caused by a defect in muscle PC biosynthesis. In addition, in *rmd* mice, hindlimb muscles are more significantly affected than forelimb muscles.¹ This is most likely explained by the fact that CHK activity is detected, though decreased, in forelimb muscles in *rmd* mice as a result of the continued post-natal expression of *Chka*.¹⁴ This indicates that the severity of muscle involvement is determined by the degree of deficiency of CHK activity.

Generally, phospholipids have saturated or monounsaturated fatty acids at the *sn-1* position and polyunsaturated fatty acids at the *sn-2* position of glycerol backbone.¹⁵ It has been shown that phospholipids have tissue-specific fatty acid composition.¹⁵ For example, heart PC and muscle PC mainly contain docosahexaenoic acid (22:6) (Nakanishi et al.¹⁵ and Figure 2C), but liver PC includes various fatty acids.¹⁵ NanoESI-MS analyses of PC molecular species in muscle and isolated mitochondria were performed with a 4000Q TRAP (AB SCIEX, Foster City, CA, USA) and a chip-based ionization source, TriVersa NanoMate (Advion BioSystems, Ithaca, NY, USA).¹⁶ Quadriceps femoris (hindlimb) and Triceps (forelimb) muscle from affected *rmd* mice and littermate controls were frozen with liquid nitrogen, and total lipid was extracted by the Blish and Dyer method.¹⁰ The ion spray voltage was set at -1.25kV, gas pressure at 0.3 pound per square inch (psi), and flow rates at 200 nl/min. The scan range was set at m/z 400~1200, declustering potential at -100V, collision energies at -35~-45V, and resolutions at Q1 and Q3 "unit." The mobile phase composition was chloroform:methanol (1/2) containing 5 mM ammonium formate and was normalized to the muscle weight. The total lipids were directly subjected by flow injection, and selectivity was analyzed by neutral loss scanning of the polar head

In muscle and isolated mitochondria, the 38:6-PC molecular species is profoundly decreased (n = 6 for muscle, n = 5 for isolated mitochondria).

Mitochondria from skeletal muscles of whole hindlimbs of *rmd* mice were isolated by the differential centrifugation method. Fresh muscle was minced and homogenized with a motor-driven Teflon pestle homogenizer with ice-cold mitochondrial isolation buffer (10 mM Tris-HCl [pH 7.2], 320 mM sucrose, 1mM EDTA, 1mM DTT, 1 mM PMSE, 1 mg/ml BSA, and protease inhibitor cocktail [Roche]) and centrifuged at 1,500 \times g for 5 min. The supernatant fraction was centrifuged at 15,000 \times g for 20 min, the pellet was resuspended in mitochondrial isolation buffer, and the centrifugation/resuspension was repeated twice more. All data are presented as means \pm standard deviation (SD). Means were compared by analysis with a two-tailed t test via R software version 2.11.0.

group for PC in negative-ion mode.¹⁷ Interestingly, there was a 10-fold decrease (9.8%) in the 16:0-22:6-PC levels versus the control in *rmd* hindlimb muscle and also in muscle mitochondria (Figure 2C), indicating the importance of the PC de novo synthesis pathway for maintaining not only PC levels but also fatty acid composition of PC molecular species. Similarly, in forelimb muscle 16:0-22:6 PC levels were also decreased in comparison to the control, but to a milder extent (18.2%), suggesting an association between severity of muscle damage and fatty acid composition alteration of PC (data not shown). In *rmd* mice, it has been shown that muscle PC can be delivered from plasma lipoprotein,¹⁸ suggesting that non-decreased PC molecular species might be derived from the plasma, whereas 16:0-22:6 PC might be synthesized only in muscle (and possibly in brain). However, confirmation of this requires further studies.

Individuals with *CHKB* mutations have severe mental retardation in addition to the muscular dystrophy. Interestingly, polymorphisms near the *CHKB* locus and decreased *CHKB* expression have been associated with narcolepsy with cataplexy, suggesting a link between *CHK-β* activity and the maintenance of normal brain function in humans.¹⁹ Furthermore, brain damage in pneumococcal infection has been attributed to the inhibition of de novo PC synthesis, suggesting the importance of PC synthesis for the brain.²⁰ Our data provide evidence that altered phospholipid biosynthesis is a causative agent for a human congenital muscular dystrophy, and further studies will elucidate the detailed molecular mechanisms of the disease in both muscle and brain.

Supplemental Data

Supplemental Data include four figures and can be found with this article online at <http://www.cell.com/AJHG/>.

Acknowledgments

We are grateful to the patients and their family for their participation, to Megumu Ogawa, Etsuko Keduca, Yuriko Kure, Mieko Ohnishi, Kaoru Tatezawa, and Kazu Iwasawa (National Center of Neurology and Psychiatry) for their technical assistance, to Naoki Kondou and Hiroyuki Taguchi (Kao Corporation) for their kind support on mass analysis, to Osamu Fujino and Kiyoshi Takahashi (Department of Pediatrics, Nippon Medical School) for providing patient information, and to Ken Inoue (National Center of Neurology and Psychiatry) for thoughtful comments on genetics. This study was supported partly by the Research on Psychiatric and Neurological Diseases and Mental Health of Health and Labour Sciences research grants; partly by Research on Intractable Diseases of Health and Labor Sciences research grants; partly by a Research Grant for Nervous and Mental Disorders (20B-12, 20B-13) from the Ministry of Health, Labour and Welfare; partly by an Intramural Research Grant (23-4, 23-5) for Neurological and Psychiatric Disorders from NCNP; partly by KAKENHI (20390250, 22791019); partly by Research on Publicly Essential Drugs and Medical Devices of Health and Labor Sciences research grants; partly by the Program for Promotion of Fundamental

Studies in Health Sciences of the National Institute of Biomedical Innovation (NIBIO); and partly by a grant from the Japan Foundation for Neuroscience and Mental Health. G.A.C. and R.B.S. were supported in part by a National Institutes of Health grant (AR-49043 to G.A.C.).

Received: March 21, 2011

Revised: April 21, 2011

Accepted: May 10, 2011

Published online: June 9, 2011

Web Resources

The URLs for data presented herein are as follows:

GenBank, <http://www.ncbi.nlm.nih.gov/Genbank>

Online Mendelian Inheritance in Man (OMIM), <http://www.omim.org>

R software version 2.11.0, <http://www.r-project.org/>

References

1. Sher, R.B., Aoyama, C., Huebsch, K.A., Ji, S., Kerner, J., Yang, Y., Frankel, W.N., Hoppel, C.L., Wood, P.A., Vance, D.E., and Cox, G.A. (2006). A rostrocaudal muscular dystrophy caused by a defect in choline kinase beta, the first enzyme in phosphatidylcholine biosynthesis. *J. Biol. Chem.* *281*, 4938–4948.
2. Nishino, I., Kobayashi, O., Goto, Y., Kurihara, M., Kumagai, K., Fujita, T., Hashimoto, K., Horai, S., and Nonaka, I. (1998). A new congenital muscular dystrophy with mitochondrial structural abnormalities. *Muscle Nerve* *21*, 40–47.
3. Hayashi, Y.K., Matsuda, C., Ogawa, M., Goto, K., Tominaga, K., Mitsuhashi, S., Park, Y.E., Nonaka, I., Hino-Fukuyo, N., Hagi-noya, K., et al. (2009). Human PTRF mutations cause secondary deficiency of caveolins resulting in muscular dystrophy with generalized lipodystrophy. *J. Clin. Invest.* *119*, 2623–2633.
4. Liao, H., Aoyama, C., Ishidate, K., and Teraoka, H. (2006). Deletion and alanine mutation analyses for the formation of active homo- or hetero-dimer complexes of mouse choline kinase- α and - β . *Biochim. Biophys. Acta* *1761*, 111–120.
5. Aoyama, C., Yamazaki, N., Terada, H., and Ishidate, K. (2000). Structure and characterization of the genes for murine choline/ethanolamine kinase isozymes alpha and beta. *J. Lipid Res.* *41*, 452–464.
6. Ishidate, K., and Nakazawa, Y. (1992). Choline/ethanolamine kinase from rat kidney. *Methods Enzymol.* *209*, 121–134.
7. Matsumoto, H., Hayashi, Y.K., Kim, D.S., Ogawa, M., Murakami, T., Noguchi, S., Nonaka, I., Nakazawa, T., Matsuo, T., Futagami, S., et al. (2005). Congenital muscular dystrophy with glycosylation defects of α -dystroglycan in Japan. *Neuromuscul. Disord.* *15*, 342–348.
8. Mitsuhashi, H., Futai, E., Sasagawa, N., Hayashi, Y., Nishino, I., and Ishiura, S. (2008). Csk-homologous kinase interacts with SHPS-1 and enhances neurite outgrowth of PC12 cells. *J. Neurochem.* *105*, 101–112.
9. Aoyama, C., Liao, H., and Ishidate, K. (2004). Structure and function of choline kinase isoforms in mammalian cells. *Prog. Lipid Res.* *43*, 266–281.
10. Bligh, E.G., and Dyer, W.J. (1959). A rapid method of total lipid extraction and purification. *Can. J. Biochem. Physiol.* *37*, 911–917.
11. Rouser, G., Fkeischer, S., and Yamamoto, A. (1970). Two dimensional thin layer chromatographic separation of polar

- lipids and determination of phospholipids by phosphorus analysis of spots. *Lipids* 5, 494–496.
12. Aoyama, C., Ohtani, A., and Ishidate, K. (2002). Expression and characterization of the active molecular forms of choline/ethanolamine kinase- α and - β in mouse tissues, including carbon tetrachloride-induced liver. *Biochem. J.* 363, 777–784.
 13. Wu, G., Aoyama, C., Young, S.G., and Vance, D.E. (2008). Early embryonic lethality caused by disruption of the gene for choline kinase alpha, the first enzyme in phosphatidylcholine biosynthesis. *J. Biol. Chem.* 283, 1456–1462.
 14. Wu, G., Sher, R.B., Cox, G.A., and Vance, D.E. (2010). Differential expression of choline kinase isoforms in skeletal muscle explains the phenotypic variability in the rostrocaudal muscular dystrophy mouse. *Biochim. Biophys. Acta* 1801, 446–454.
 15. Nakanishi, H., Iida, Y., Shimizu, T., and Taguchi, R. (2010). Separation and quantification of sn-1 and sn-2 fatty acid positional isomers in phosphatidylcholine by RPLC-ESIMS/MS. *J. Biochem.* 147, 245–256.
 16. Ikeda, K., Mutoh, M., Teraoka, N., Nakanishi, H., Wakabayashi, K., and Taguchi, R. (2011). Increase of oxidant-related triglycerides and phosphatidylcholines in serum and small intestinal mucosa during development of intestinal polyp formation in Min mice. *Cancer Sci.* 102, 79–87.
 17. Taguchi, R., Houjou, T., Nakanishi, H., Yamazaki, T., Ishida, M., Imagawa, M., and Shimizu, T. (2005). Focused lipidomics by tandem mass spectrometry. *J. Chromatogr. B Analyt. Technol. Biomed. Life Sci.* 823, 26–36.
 18. Wu, G., Sher, R.B., Cox, G.A., and Vance, D.E. (2009). Understanding the muscular dystrophy caused by deletion of choline kinase beta in mice. *Biochim. Biophys. Acta* 1791, 347–356.
 19. Miyagawa, T., Kawashima, M., Nishida, N., Ohashi, J., Kimura, R., Fujimoto, A., Shimada, M., Morishita, S., Shigeta, T., Lin, L., et al. (2008). Variant between CPT1B and CHKB associated with susceptibility to narcolepsy. *Nat. Genet.* 40, 1324–1328.
 20. Zweigner, J., Jackowski, S., Smith, S.H., Van Der Merwe, M., Weber, J.R., and Tuomanen, E.I. (2004). Bacterial inhibition of phosphatidylcholine synthesis triggers apoptosis in the brain. *J. Exp. Med.* 200, 99–106.

Muscle choline kinase beta defect causes mitochondrial dysfunction and increased mitophagy

Satomi Mitsuhashi¹, Hideyuki Hatakeyama², Minako Karahashi³, Tomoko Koumura³, Ikuya Nonaka¹, Yukiko K. Hayashi¹, Satoru Noguchi¹, Roger B. Sher⁴, Yasuhito Nakagawa³, Giovanni Manfredi⁵, Yu-ichi Goto², Gregory A. Cox⁴ and Ichizo Nishino^{1,*}

¹Department of Neuromuscular Research and ²Department of Mental Retardation and Birth Defect Research, National Institute of Neuroscience, National Center of Neurology and Psychiatry, Tokyo, Japan, ³School of Pharmaceutical Sciences, Kitasato University, Tokyo, Japan, ⁴The Jackson Laboratory, Bar Harbor, ME, USA and ⁵Weil Medical College of Cornell University, New York, NY, USA

Received May 17, 2011; Revised and Accepted July 7, 2011

Choline kinase is the first step enzyme for phosphatidylcholine (PC) *de novo* biosynthesis. Loss of choline kinase activity in muscle causes rostrocaudal muscular dystrophy (*rmd*) in mouse and congenital muscular dystrophy in human, characterized by distinct mitochondrial morphological abnormalities. We performed biochemical and pathological analyses on skeletal muscle mitochondria from *rmd* mice. No mitochondria were found in the center of muscle fibers, while those located at the periphery of the fibers were significantly enlarged. Muscle mitochondria in *rmd* mice exhibited significantly decreased PC levels, impaired respiratory chain enzyme activities, decreased mitochondrial ATP synthesis, decreased coenzyme Q and increased superoxide production. Electron microscopy showed the selective autophagic elimination of mitochondria in *rmd* muscle. Molecular markers of mitophagy, including Parkin, PINK1, LC3, polyubiquitin and p62, were localized to mitochondria of *rmd* muscle. Quantitative analysis shows that the number of mitochondria in muscle fibers and mitochondrial DNA copy number were decreased. We demonstrated that the genetic defect in choline kinase in muscle results in mitochondrial dysfunction and subsequent mitochondrial loss through enhanced activation of mitophagy. These findings provide a first evidence for a pathomechanistic link between *de novo* PC biosynthesis and mitochondrial abnormality.

INTRODUCTION

Phosphatidylcholine (PC) is the major phospholipid in eukaryotic cell membranes. Disruption of PC synthesis by loss-of-function mutations in *CHKB* (GenBank Gene ID 1120), which encodes the primary choline kinase isoform in muscle, causes autosomal recessive congenital muscular dystrophy with mitochondrial structural abnormalities in human (1). Loss-of-function mutation in the murine ortholog, *Chkb*, is reported to cause rostrocaudal muscular dystrophy (*rmd*) in the laboratory mouse (2). *Rmd* is so-named because of a gradient of severity of muscle damage—hindlimbs (caudal)

are affected more severely than forelimbs (rostral). The most outstanding feature of the muscle pathology in both human patients and *rmd* mice is a peculiar mitochondrial abnormality—mitochondria are greatly enlarged at the periphery of the fiber and absent from the center.

Mitochondria have a variety of cellular functions from energy production to triggering apoptotic cell death (3,4). Inhibition of mitochondrial respiration [chemically or by mitochondrial DNA (mtDNA) mutations], disruption of inner membrane potential, senescence and enhanced reactive oxygen species (ROS) production are all known to cause mitochondrial morphological abnormalities (5–8). Conversely,

*To whom correspondence should be addressed at: Department of Neuromuscular Research, National Institute of Neuroscience, National Center of Neurology and Psychiatry, 4-1-1 Ogawahigashi-cho, Kodaira, Tokyo 187-8502, Japan. Tel: +81 423461712; Fax: +81 423461742; Email: nishino@ncnp.go.jp

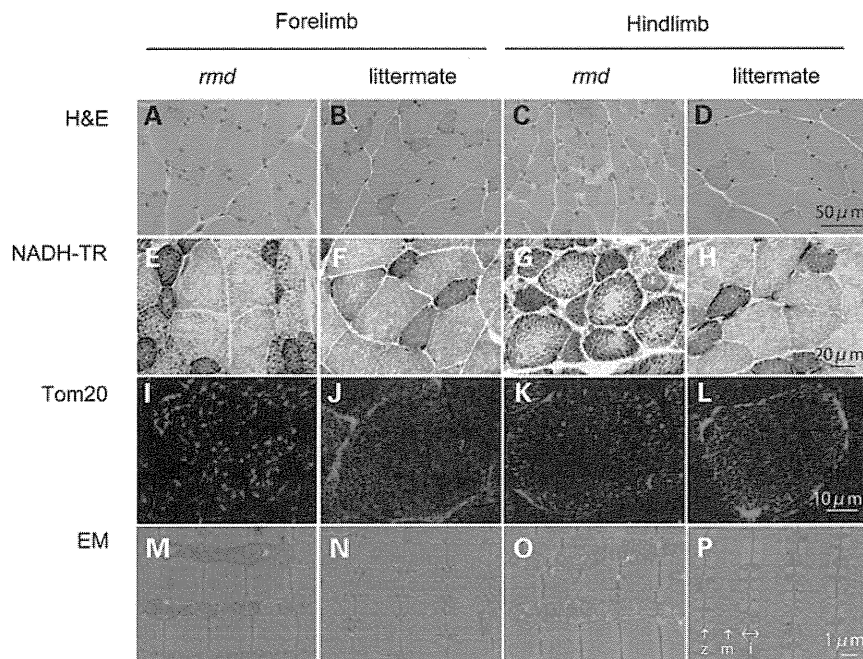


Figure 1. Muscle histopathology. H&E staining of triceps or quadriceps femoris muscles in 8-week-old homozygous *rmd* mutant mice and unaffected (+/*rmd* or +/+) littermate controls (A–D) shows dystrophic changes including variation in fiber size, necrosis and regeneration of individual fibers and interstitial fibrosis. NADH-TR staining (E–H), immunostaining of mitochondrial outer membrane protein Tom20 and EM (M–P) show abnormal mitochondria. Mitochondria in *rmd* muscle fibers are enlarged and prominent at the periphery, but sparse in the center (I–L). z, Z line; m, M line; i, I band.

primary mitochondrial morphological changes can subsequently cause mitochondrial and cellular dysfunction. Mitochondria are dynamic organelles, which continuously fuse and divide. Disequilibrium of mitochondrial fusion and fission can cause alterations of mitochondrial morphology with mitochondrial dysfunction (9,10). Thus, mitochondrial function and morphology are tightly linked.

It has been reported that mitochondria in *rmd* show decreased membrane potential (11). However, there have been no further studies about mitochondrial functional abnormalities in *rmd*, although its morphology is the most distinct feature compared with other myopathies. In addition, there has been no study about mitochondrial function when PC synthesis is blocked *in vivo*, although mitochondrial respiratory enzyme activities are dependent on membrane phospholipids (12). We hypothesized that the mitochondrial morphological abnormality in *rmd* muscle indicates the presence of a bioenergetic dysfunction caused by mitochondrial membrane phospholipid alteration.

In this study, we demonstrate that mitochondria in *rmd* mouse muscle show reduced PC level, bioenergetic dysfunction and increased ROS production are ubiquitinated and eliminated via mitophagy, leading to the peculiar mitochondrial loss in the skeletal muscle. These findings provide further evidence that mitochondrial dysfunction is related to phospholipid metabolism and may play a role in the pathogenesis of muscle disease.

RESULTS

Light microscopic examination of H&E-stained samples from 8-week-old homozygous *rmd* mutant mice and littermate

controls confirmed dystrophic muscle pathology, especially in hindlimb muscles, as previously described (2) (Fig. 1A–D). NADH-TR and immunohistochemistry for mitochondrial outer membrane protein Tom20 also showed that mitochondria were sparse in the muscle fiber both in forelimb and hindlimb muscles of *rmd* mice, while the remaining mitochondria were prominent (Fig. 1E–L). More striking is the mitochondrial enlargement observed by EM (Fig. 1M–P). Mitochondria were rounder and massively enlarged compared with littermate controls. Normally, two mitochondria are present in almost all intermyofibrillar spaces and extend alongside the region between Z band and I bands. In muscles of *rmd* mice, mitochondria were larger than the size of the Z-I length itself, and often exceeded the size of a single sarcomere. In addition, mitochondria were seen only in some intermyofibrillar spaces leaving many regions devoid of mitochondria.

We hypothesized that the abnormal mitochondrial morphology in *rmd* skeletal muscles reflects altered PC content in mitochondrial membranes, as these mitochondria lack the PC biosynthetic pathway. We therefore measured PC, PE and CL in isolated mitochondria (Fig. 2). PE is the second most abundant phospholipid in mitochondria and CL is a mitochondria-specific phospholipid. PC was significantly decreased to 72% in forelimb and to 61% in hindlimb muscles compared with healthy littermates, while PE levels were unchanged. The PC/PE ratio was decreased, reflecting the PC reduction. This reduction is well correlated with the phospholipid compositional alteration in muscle tissue as previously described (1,2). CL showed only a slight decrease and only in the more severely affected hindlimb muscles.

We speculated that mitochondrial function in *rmd* is altered, and therefore measured respiratory enzyme activity and ATP

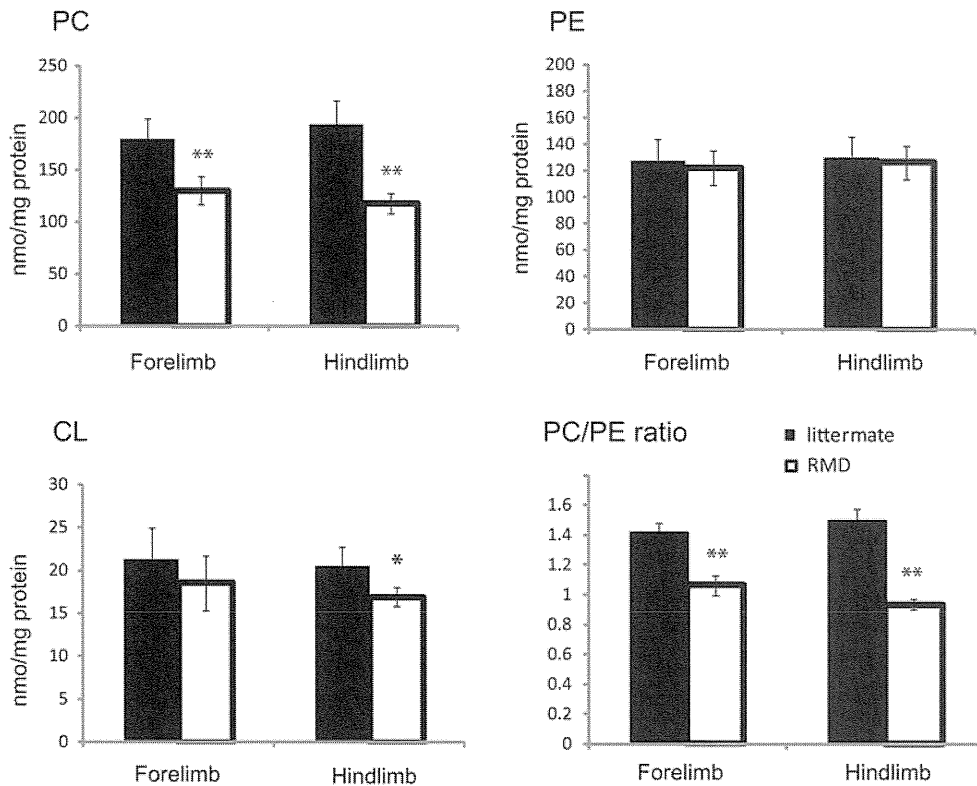


Figure 2. The PC level is decreased in *rmd* muscle mitochondria. The PE level is not altered. The PC/PE ratio is significantly decreased in *rmd*. The CL level is slightly decreased in *rmd* hindlimb. Data are expressed as the mean \pm SD of eight experiments. * $P < 0.01$, ** $P < 0.0001$.

synthesis in isolated mitochondria in *rmd* muscle. Compared with healthy littermates, only mitochondrial respiratory Complex III activity was significantly decreased in mitochondria from *rmd* forelimb muscles, while Complex I, III and IV activities were significantly decreased in *rmd* hindlimb muscles (Fig. 3A). Mitochondrial ATP synthesis was severely decreased, especially in hindlimb muscles (Fig. 3B), and coenzyme Q9 was moderately decreased in *rmd* compared with littermates (Fig. 3C).

In-gel activity staining on native PAGE showed decreased Complex III activity, especially in hindlimb (Fig. 4A), although normal protein levels of the Complex III were detected by western blot followed by Native PAGE (Fig. 4B). There was no difference in mobility of Complex III in *rmd* and littermate. Furthermore, respiratory chain supercomplex formation, which is important for effective electron transport (24), was not altered in *rmd* (Supplementary Material, Fig. S1).

Mitochondria are a major site of ROS production under normal circumstances and the production of ROS is enhanced when respiration is blocked. To determine whether the identified respiratory defects lead to elevated ROS, we measured superoxide levels from isolated mitochondria. Superoxide production was significantly increased in *rmd* muscle mitochondria, especially in those isolated from the hindlimbs (Fig. 5A). Moreover, the MDA level (Fig. 5B) and 4-hydroxynonenal adducts (Fig. 5C) were increased in *rmd* muscles indicating that oxidative stress is increased in *rmd* muscle.

Interestingly, examination of muscle sections by EM revealed autophagosomes selectively engulfing an entire mitochondrion, without cytoplasm, suggesting that mitophagy is activated in *rmd* skeletal muscles (Fig. 6A). Western blots of isolated mitochondria from muscle showed significantly increased levels of the autophagosome marker LC3 in *rmd* (Fig. 6B). In addition, polyubiquitinated proteins and p62/SQSTM1, which connects ubiquitination and autophagic machineries, were also increased in isolated mitochondria (Fig. 6B). These data suggest that mitochondria are polyubiquitinated and p62 is recruited to mitochondria. We also analyzed PINK1 and the E3 ubiquitin ligase Parkin, which are known to contribute to ubiquitination and mitophagy of damaged mitochondria (25,26). PINK1 and Parkin levels were increased in *rmd* isolated muscle mitochondria (Fig. 6B), suggesting that they were recruited to mitochondria to promote mitophagy. Immunohistochemical analyses demonstrated the colocalization of p62, polyubiquitin and LC3 with mitochondria (Fig. 6C).

We quantified mitochondrial numbers in muscle fibers, mitochondria occupying-area relative to muscle cross-sectional area and mean mitochondrial area in cross-section by morphometric analysis in EM. In *rmd*, the average number of mitochondria per fiber was profoundly decreased (Fig. 7A). However, the average area occupied by mitochondria in each muscle fiber was comparable with littermates (Fig. 7A). This was due to increased mean mitochondrial area in *rmd* (Fig. 7A).

We quantified mtDNA copy number relative to nuclear DNA. In *rmd*, mtDNA was decreased both in forelimb and

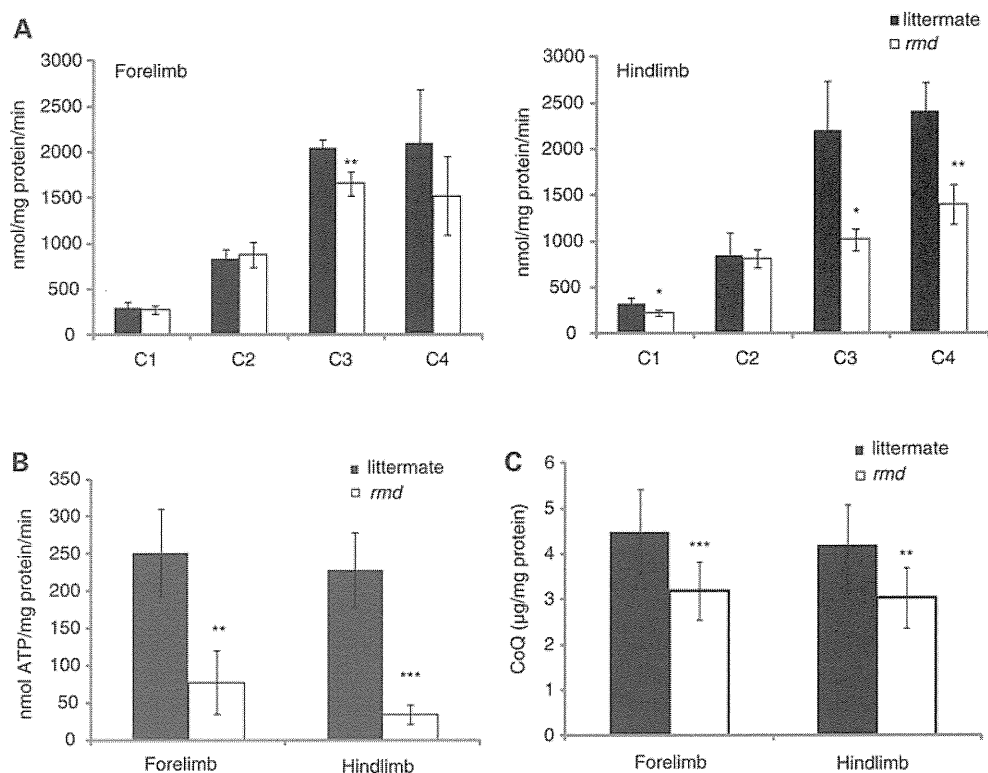


Figure 3. Mitochondrial energetic function is altered and CoQ level is decreased in *rmd*. (A) Mitochondrial respiratory chain enzyme activities in *rmd* were compared with healthy littermates. C1, Complex I ; C2, Complex II ; C3, Complex III ; C4, Complex IV ($n = 4$). (B) The rate of ATP synthesis measured by luminometry method ($n = 4$). (C) Total CoQ9 level (littermate forelimb, $n = 13$; littermate hindlimb, $n = 12$; *rmd* forelimb, $n = 11$; *rmd* hindlimb, $n = 13$). Data are expressed as the mean \pm SD of experiment number shown as n . * $P < 0.05$, ** $P < 0.005$, *** $P < 0.001$.

hindlimb muscles compared with littermate controls (Fig. 7B), which was in agreement with the number of mitochondria decrease. The mtDNA copy number in liver is preserved in *rmd*, and reduction in muscle is progressive in age.

DISCUSSION

In the *rmd* mouse, we observed greater superoxide production and more significant Complex III and ATP synthesis deficiencies in hindlimb than in forelimb muscles, correlating with the more severe caudal phenotype. PC was decreased in isolated *rmd* muscle mitochondria as a consequence of disruption of muscle PC biosynthesis because PC cannot be synthesized in mitochondria. This suggests that muscle damage in the *rmd* mouse is primarily due to mitochondrial dysfunction possibly caused by the impaired PC biosynthesis.

Why then are mitochondrial functions altered when PC is decreased? Mitochondria produce energy mainly via oxidative phosphorylation, which transfers electrons by a series of redox reactions through four enzyme complexes, and pumps protons across the mitochondrial inner membrane, producing an electrochemical proton gradient that enables ATP synthesis (3). Here, we demonstrate for the first time a Complex III activity decrease without the loss of the enzyme protein complex in *rmd* muscle mitochondria, suggesting a link between decreased PC content and Complex III activity. One possible explanation is that mitochondrial PC alterations may directly impair Complex III function by affecting lipid-protein

interactions (27). PC is a component of the yeast respiratory enzyme complex, as revealed by X-ray crystallography, and thus may regulate enzyme function (28). Alteration of fatty acid composition in PC has been shown to change enzymatic activity in Complexes I, III and IV in a mouse model (29). In this model, Complex III activity is profoundly increased when n-3 fatty acid is increased. In *rmd*, it is reported that docosahexaenoic acid containing PC, the major n-3 fatty acid in muscle PC, is profoundly decreased in muscle and in isolated mitochondria (1). This suggests a possible association between phospholipid composition alterations and respiratory chain enzymatic activities due to the choline kinase defect in *rmd* muscle.

Through the oxidative phosphorylation process, ROS are also generated as byproducts even in normal cellular states, but especially when respiration is inhibited (30,31). In *rmd* mouse muscle, ROS production from isolated mitochondria was increased, which may be related to the respiratory chain defect caused by PC reduction in mitochondria. Interestingly, selenium-deficient myopathy is associated with muscle pathology showing similar enlarged and sparse mitochondrial morphological abnormalities to the *rmd* mice and the human congenital muscular dystrophy caused by *CHKB* mutations (32). As selenium is a cofactor of glutathione peroxidase, selenium deficiency is thought to cause oxidative stress (33,34). Morphological similarity between choline kinase beta deficiency and selenium deficiency suggests that ROS may play a key role in the formation of the mitochondrial

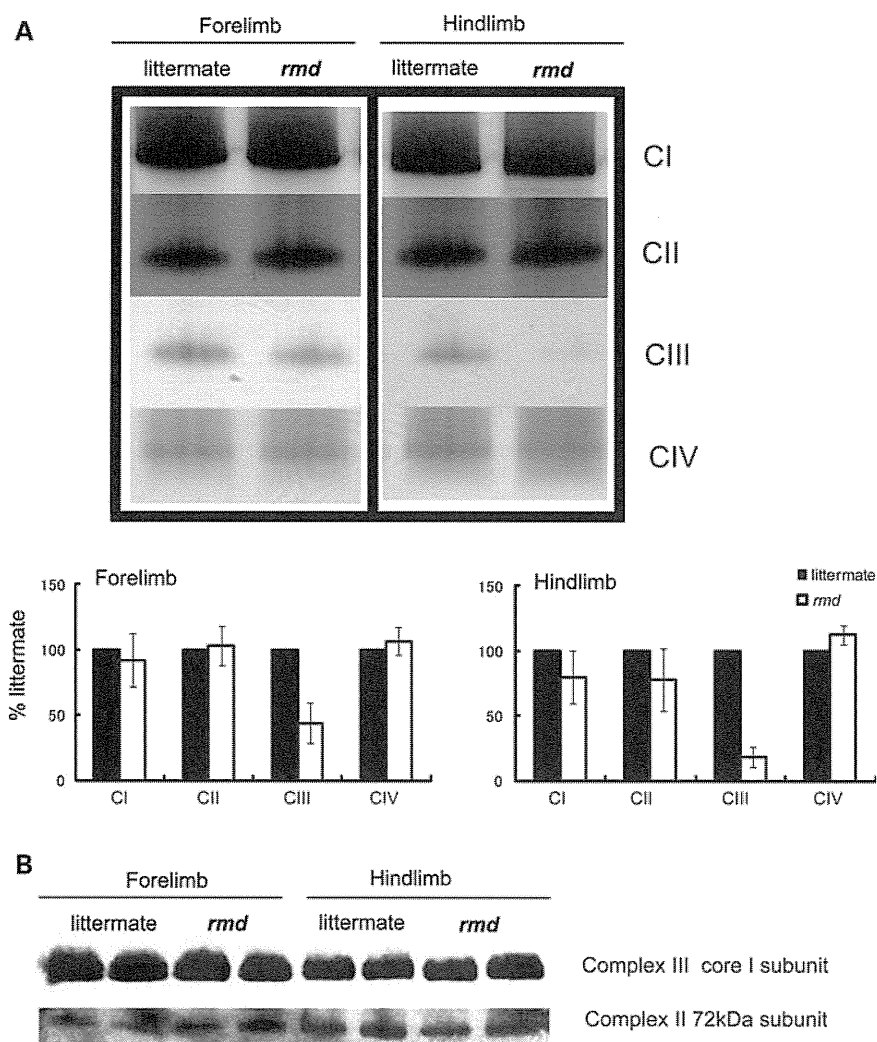


Figure 4. Mitochondrial respiratory enzyme activity is decreased without the loss of the enzyme complex. (A) Native PAGE gel electrophoresis. In-gel activity staining shows that Complex III activity is decreased in *rmd*. Representative data from four different experiments are shown. (B) Immunoblotting of Complex II and III shows protein levels are maintained despite defect in significant Complex III enzymatic activity. Representative data from three different experiments of six samples are shown.

abnormalities in *rmd* myopathy. In another model, depletion of glutathione, which provides cells with a reducing environment and detoxifies the ROS, is reported to cause mitochondria enlargement in muscle, also suggesting the possible link between mitochondrial enlargement and ROS in skeletal muscle (35).

In addition, as a major site of ROS production, mitochondria themselves are prone to ROS damage (36). Recent studies have shown that damaged mitochondria are eliminated by selective autophagy, called mitophagy, most likely as a quality control mechanism to protect the cells (37,38). In addition to mitochondrial enlargement, we observed large areas devoid of mitochondria. Mitochondrial depolarization can trigger mitophagy in cell culture models (26). PINK1 and Parkin interactions promote ubiquitination of mitochondrial outer membrane proteins, and induce mitophagy. This process is mediated by p62, an adaptor molecule, which interacts directly with ubiquitin and LC3 (25,39). ROS generated from mitochondria are also important for mitophagy (39).

Interestingly, we found increased mitophagy in *rmd*, accompanied by mitochondrial ubiquitination and recruitment of p62 and LC3. Enhanced PINK1 and Parkin expression in mitochondria likely reflects the process of elimination of damaged mitochondria as a consequence of mitochondrial dysfunction and ROS production. These findings were similar to those in cells treated with the protonophore carbonyl cyanide *m*-chlorophenyl hydrazone (CCCP) or respiratory chain inhibitors (25,26). In *rmd*, decreased membrane potential (11), as a consequence of respiratory chain insufficiency and ROS production, may trigger mitophagy and thus increased mitochondrial clearance, which may lead to energy crisis and result in cell death and muscular dystrophy.

We observed progressive loss of mtDNA with age, together with progressive loss of mitochondria. We suggest that mtDNA depletion in this case results from increased mitophagy, because mtDNA is known to be degraded by mitophagy in cultured hepatocytes (40) and because the pathological features of CHKB-deficient myopathy are clearly distinct from those

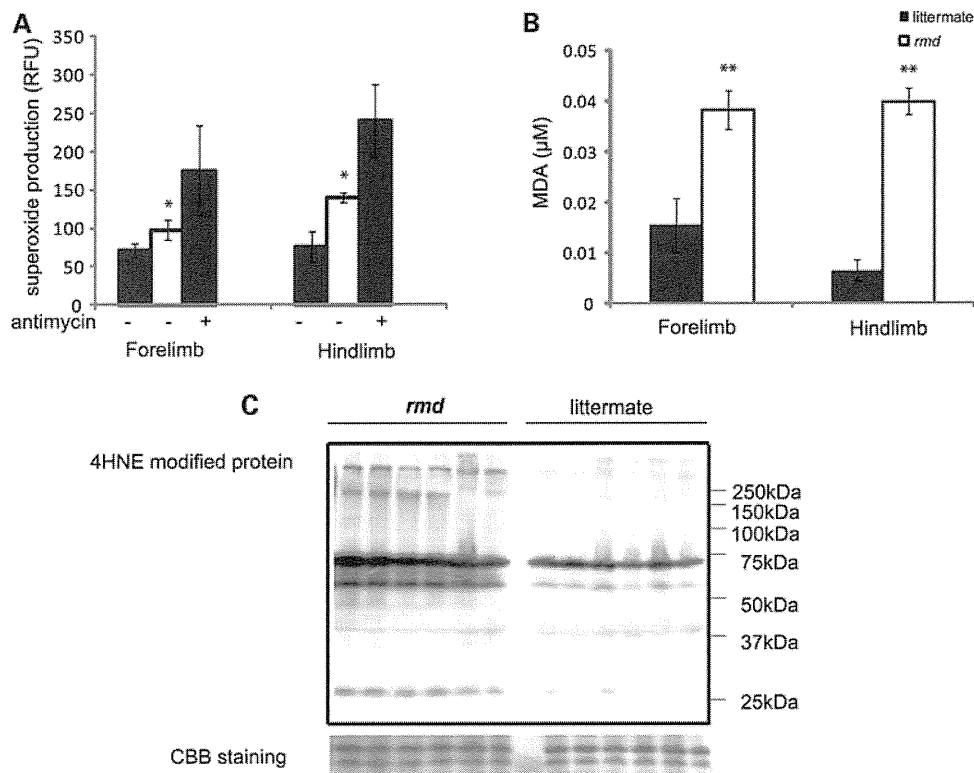


Figure 5. Mitochondrial superoxide production is increased and oxidative stress is increased in muscle tissue in *rmd*. (A) Mitochondrial superoxide production is enhanced in *rmd*, especially in hindlimb muscle mitochondria. Data are shown as the mean \pm SD of seven experiments. * $P < 0.001$. (B) MDA levels are increased in muscle tissue. ** $P < 0.0005$. Data are shown as the mean \pm SD ($n = 4$ for *rmd* and $n = 5$ for littermate controls). (C) HNE4-modified proteins are increased in *rmd* hindlimb muscle. Coomassie brilliant blue staining is shown as a loading control. Representative data of six samples.

observed in 'primary' mtDNA depletion syndromes, usually associated with defective mtDNA synthesis, in which muscle fiber mitochondria are increased both in number and size, causing the 'ragged-red fiber' appearance (41).

In summary, we have demonstrated for the first time a pathogenic mechanism that links PC reduction in the mitochondrial membranes of *rmd* muscle to mitochondrial morphological and functional abnormalities and the induction of mitophagy as a response to structural and functional damage by ROS generation or impaired bioenergetics. These findings indicate the importance of PC *de novo* synthesis pathway and phospholipid composition of mitochondrial membrane in the maintenance of mitochondria and muscle.

MATERIALS AND METHODS

Rmd mice

Eight-week-old *rmd* mice (2) were used for all analysis and were compared with healthy littermates. The Ethical Review

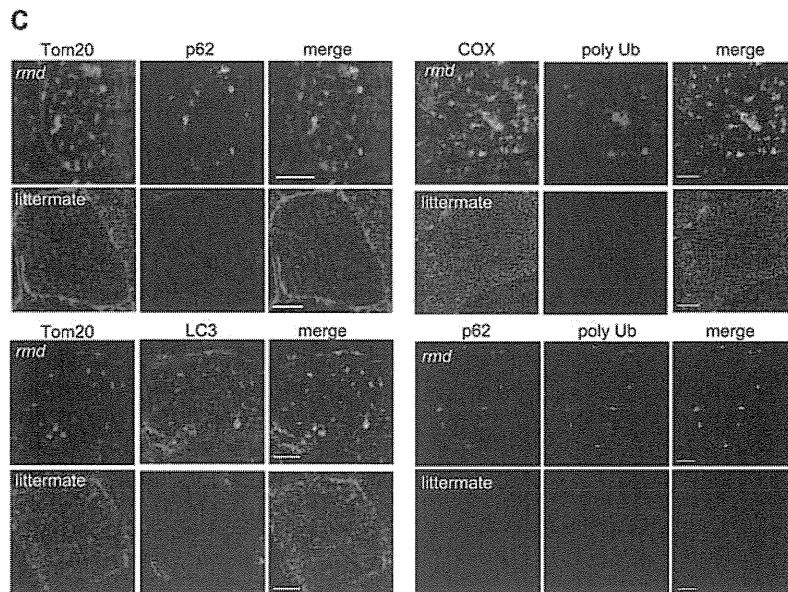
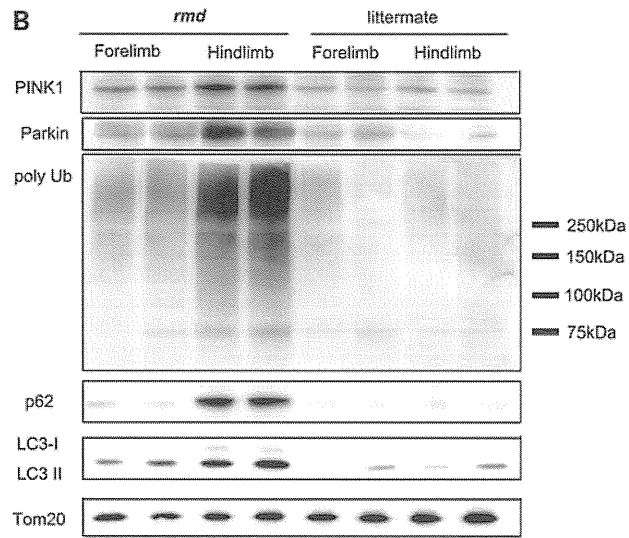
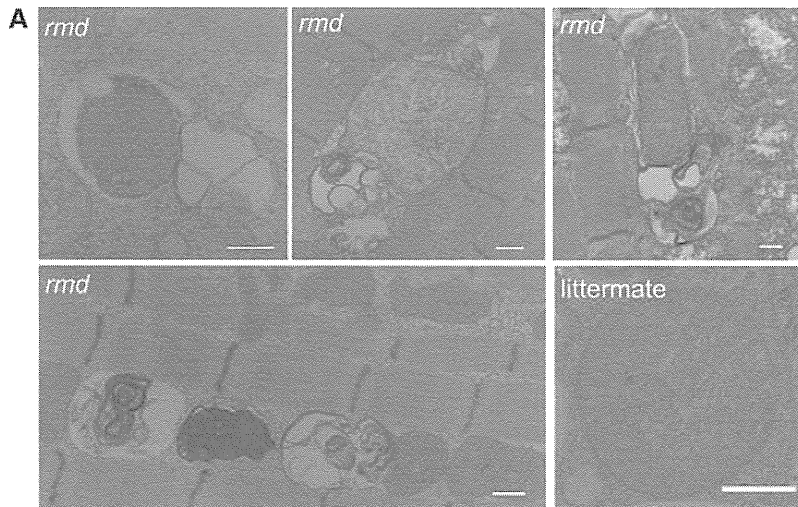
Committee on the Care and Use of Rodents in the National Institute of Neuroscience, National Center of Neurology and Psychiatry approved all mouse experiments.

Histological analyses

The quadriceps femoris muscles were freeze-fixed in liquid-nitrogen-cooled isopentane and stored at -80°C . Serial transverse sections of 10 μm thickness were stained with a series of histochemical methods, including hematoxylin and eosin (H&E) and nicotine amide adenine dinucleotide-tetrazolium reductase (NADH-TR), as previously described (13), and were observed by light microscopy.

Immunohistochemical analyses were performed as previously described (13). Briefly, 6 μm thick frozen muscle sections were fixed in cold acetone for 5 min. After blocking with 5% normal goat serum, sections were incubated with primary antibodies for 2 h at 37°C . After rinses with phosphate-buffered saline, sections were incubated with secondary Alexa Fluor 488- or Alexa Fluor 568-labeled goat anti-mouse

Figure 6. Mitochondrial degeneration in *rmd*. (A) EM of extensor digitorum longus muscle. In *rmd*, mitochondria are degraded by mitophagy. Scale bar = 0.5 μm . (B) Western blot of isolated muscle mitochondria immunodetected for Parkin, polyubiquitin, p62/SQSTM1 and LC3. TOM20, a mitochondrial outer membrane protein is used as loading control. Hindlimb mitochondria in *rmd* show significantly increased expression level in these mitophagy markers. (C) p62 and TOM20 immunohistochemistry of hindlimb muscle section. Note that mitochondria are significantly enlarged and sparse in *rmd*. p62 colocalizes with the mitochondrial outer membrane protein TOM20. Polyubiquitin and mitochondrial protein cytochrome c oxidase (COX) colocalize. LC3 and TOM20 colocalize. Polyubiquitin and p62 colocalize. Scale bar = 10 μm .



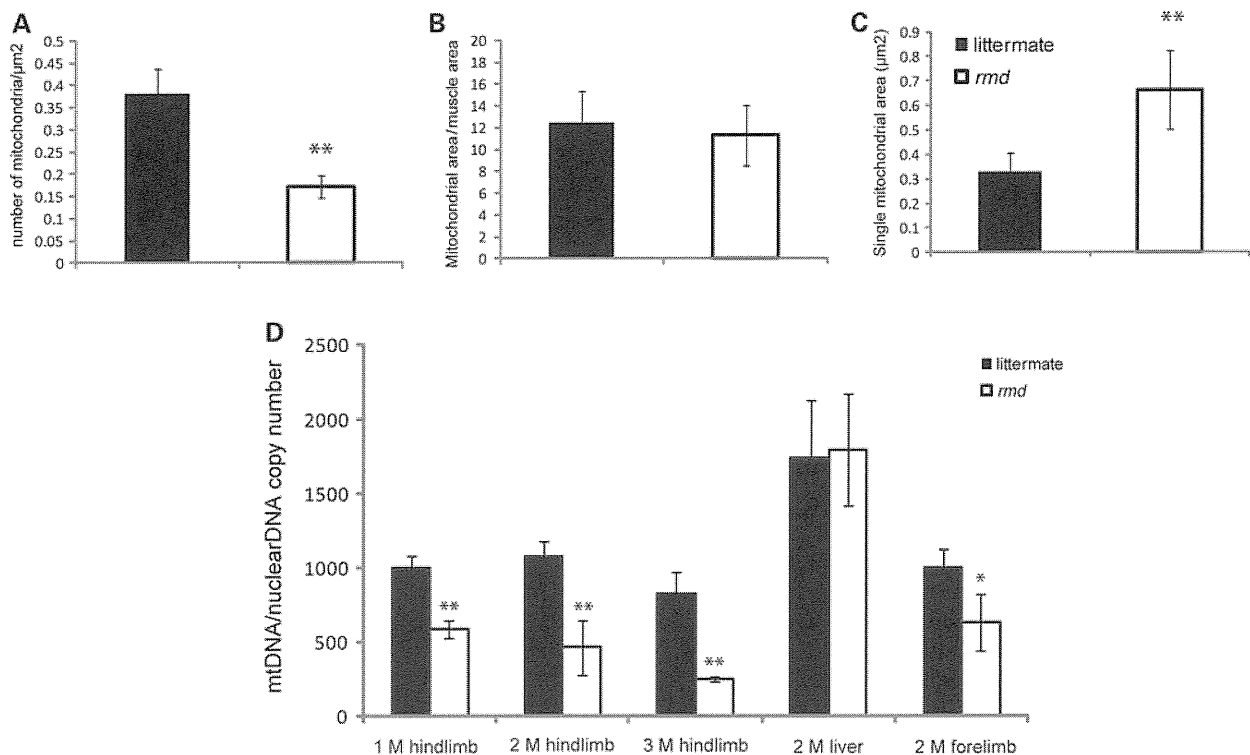


Figure 7. (A) Mitochondrial morphometrical analysis. All mitochondria are counted in cross-sections of EDL muscle by EM. Number of mitochondria per $1 \mu\text{m}^2$ of muscle fiber cross-sectional area is shown ($n = 20$). The percentage of area occupied by mitochondria in a cross-section of muscle fiber is not different in *rmd* and littermates ($n = 20$). The average total mitochondrial area per muscle fiber is larger in *rmd* compared with littermates ($n = 20$). $*P < 0.005$, $**P < 0.0005$. (B) mtDNA copy number is decreased in *rmd* compared with littermate controls. Copy number of mtDNA (ND1) was normalized by nuclear DNA (*pcam1*) (M; month-old, 1 M hindlimb: *rmd*; $n = 4$, littermates; $n = 4$. 2 M hindlimb: *rmd*; $n = 5$, littermates; $n = 6$, 3 M hindlimb: *rmd*; $n = 4$, littermates; $n = 6$. 2 M liver: *rmd*; $n = 5$, littermates; $n = 5$. 2 M forelimb: *rmd*; $n = 6$, littermates; $n = 6$).

or rabbit antibodies at room temperature for 45 min. Confocal images were obtained with FLUOVIEW FV500 systems (Olympus) using a $\times 100$ objective.

For observation by electron microscopy (EM), muscle samples were fixed in 2.5% glutaraldehyde in 0.1 M cacodylate buffer. Specimens were post-fixed in 1% osmium tetroxide in the same buffer, dehydrated with graded series of ethanol and embedded in epon, as previously described (13). Ultrathin sections were stained with uranyl acetate and lead citrate, and were analyzed by a FEI Tecnai Spirit at 120 kV.

Isolation of skeletal muscle mitochondria

Mitochondria from skeletal muscle of whole forelimb and hindlimbs were isolated by differential centrifugation. Fresh muscle was minced and homogenized using a motor-driven Teflon pestle homogenizer with ice-cold mitochondrial isolation buffer [10 mM Tris-HCl pH 7.2, 320 mM sucrose, 1 mM ethylenediaminetetraacetic acid, 1 mM dithiothreitol, 1 mg/ml bovine serum albumin (BSA)] and centrifuged at 1500g for 5 min. Supernatant fraction was centrifuged at 15 000g for 20 min, and the pellet was resuspended in mitochondrial isolation buffer. The centrifugation was repeated twice. Protein concentration was determined by the Bradford method using Bio-Rad Protein Assay (Bio-Rad Laboratories), according to the manufacturer's protocol.

Lipid extraction, phospholipid separation and determination

PC, phosphatidylethanolamine (PE) and cardiolipin (CL) were extracted from isolated mitochondria of forelimb and hindlimb muscles, separated by one-dimensional thin layer chromatography (TLC) and amount of each phospholipid was measured by phosphorus analysis (14,15). Briefly, total lipids in frozen muscle biopsy samples were extracted according to the method of Bligh and Dyer (14). Each extract was evaporated to dryness under nitrogen, and the residues were then dissolved in a small amount of a 2:1 v/v mixture of chloroform and methanol and applied to a TLC plate (Merck, Silica Gel 60). The plate was developed with a medium of chloroform:methanol:formic acid:acetic acid = 100:100:9:9 (v/v/v/v). The products and standards were visualized with primulin reagent, and the products identified by comparison with chromatographic standards. PC and PE were then scraped from the TLC plate for quantification. Phospholipids were quantified according to the method of Rouser *et al.* (15). Briefly, the lipids were digested by heating for 1 h at 200°C with 70% perchloric acid. After cooling, ammonium molybdate and ascorbic acid solution were added in that order. Color was developed after heating for 5 min in a boiling water bath. Absorbance was determined at 820 nm by spectrophotometer. Phospholipid levels were corrected by the total protein amount in isolated mitochondria.

Respiratory enzyme activity and ATP synthesis

Mitochondrial respiratory enzyme activities were measured as previously described, using colorimetric assays in isolated mitochondria (16,17). Complex I (NADH-ubiquinone oxidoreductase) activity was measured by the reduction of $10\ \mu\text{M}$ decylubiquinone (DB) in the presence of $2\ \text{mM}$ potassium cyanide (KCN), $50\ \mu\text{g/ml}$ antimycin and $50\ \mu\text{M}$ NADH at $272\ \text{nm}$. Complex II (succinate-ubiquinone oxidoreductase) activity was measured by the reduction of $50\ \mu\text{M}$ 2,6-dichlorophenolindophenol in the presence of $20\ \text{mM}$ succinate, $2.5\ \mu\text{g/ml}$ rotenone, $2.5\ \mu\text{g/ml}$ antimycin, $2\ \text{mM}$ KCN and $50\ \mu\text{M}$ DB at $600\ \text{nm}$. Complex III (ubiquinol-ferricytochrome c oxidoreductase) activity was measured by the reduction of $50\ \mu\text{M}$ cytochrome c at $550\ \text{nm}$ in the presence of $50\ \mu\text{M}$ reduced DB and $2\ \text{mM}$ KCN. Complex IV (ferrocytochrome c-oxigen oxidoreductase) activity was measured by the oxidation of $2.5\ \mu\text{M}$ reduced cytochrome c at $550\ \text{nm}$. The activity was calculated using an extinction coefficient of $8\ \text{mM}^{-1}\ \text{cm}^{-1}$, $19.1\ \text{mM}^{-1}\ \text{cm}^{-1}$, $19.0\ \text{mM}^{-1}\ \text{cm}^{-1}$ and $19.0\ \text{mM}^{-1}\ \text{cm}^{-1}$ for Complexes I, II, III and IV, respectively. The specific activity of the enzymes was expressed as nmol of each substrate oxidized or reduced/min/mg of mitochondrial protein.

Mitochondrial ATP synthesis was measured by the method of Manfredi and colleagues (18). Briefly, isolated mitochondria were resuspended in $0.25\ \text{M}$ sucrose, $50\ \text{mM}$ 4-(2-hydroxyethyl)-1-piperazineethanesulfonic acid (HEPES), $2\ \text{mM}$ MgCl_2 , $1\ \text{mM}$ ethylene glycol tetraacetic acid (EGTA) and $10\ \text{mM}$ KH_2PO_4 , pH 7.4. Then $0.15\ \text{mM}$ P1,P5-di(adenosine) pentaphosphate, $1\ \text{mM}$ malate, $1\ \text{mM}$ pyruvate, luciferin and luciferase and $0.1\ \text{mM}$ adenosine diphosphate (ADP) were added, and light emission was recorded by luminometer. For each sample, $1\ \text{mM}$ oligomycin-added sample was used to obtain the baseline luminescence corresponding to non-mitochondrial ATP production.

CoQ9 determination

Total CoQ9 contents in isolated mitochondria were analyzed with high performance liquid chromatography (HPLC) by electrochemical detection according to the standard procedure described by Tang *et al.* (19). Briefly, isolated muscle mitochondria pellet were lysed with 2-propanol, vortexed for 1 min and centrifuged at $2000g$ for 10 min and then clear supernatant was applied for HPLC Coul Array Detector Model 5600A (ESA BIOSCIENCES, Inc.) with Capcell Pak C18 MG 100 column ($3.2\ \text{I.D.} \times 150\ \text{mm}$ length; ESA BIOSCIENCES, Inc.). The mobile phase was degassed methanol containing 0.4% sodium acetate, 1.5% acetic acid, 1% 2-propanol and 8% n-hexane. Chromatographic data were analyzed with CoulArray Data Station 3.00 (ESA Biosciences). Standard curves were created with both oxidized and reduced CoQ9. Total CoQ9 level was determined according to the standard curve and corrected by the total protein level in isolated mitochondria as measured by the Bradford method.

High-resolution clear native PAGE

High-resolution clear native polyacrylamide gel electrophoresis (PAGE) was performed by the method of Wittig *et al.*

(20). Briefly, isolated mitochondria were solubilized with Native PAGE Sample buffer (Invitrogen) containing 0.3% n-dodecyl- β -D-maltoside (Dojindo). Twenty micrograms of protein were applied to 3–12% NativePAGE Bis-Tris gel (Invitrogen). Native PAGE buffer (Invitrogen) was used for anode buffer and Native PAGE buffer containing 0.02% n-dodecyl- β -D-maltoside and 0.05% deoxycolate was used for cathode buffer.

For in-gel catalytic activity assays, gels were incubated in the following solutions: Complex I, $5\ \text{mM}$ Tris-HCl pH 7.4, $140\ \mu\text{M}$ NADH and $3\ \text{mM}$ nitro tetrazolium blue (NTB); Complex II, $5\ \text{mM}$ Tris-HCl pH 7.4, $20\ \text{mM}$ succinate, $3\ \text{mM}$ NTB and $200\ \mu\text{M}$ phenazine methosulfate; Complex III, $50\ \text{mM}$ sodium phosphate buffer pH 7.2 and $0.5\ \text{mg/ml}$ diaminobenzidine (DAB); Complex IV, $50\ \text{mM}$ sodium phosphate buffer (pH 7.2), $0.5\ \text{mg/ml}$ DAB and $5\ \text{mM}$ cytochrome c.

For immunoblotting, gels were incubated for 20 min in $300\ \text{mM}$ Tris, $100\ \text{mM}$ acetic acid, 1% sodium dodecyl sulfate (SDS), pH 8.6 and then electroblotted to polyvinylidene fluoride (PVDF) membrane (Millipore). Complexes II and III were detected with monoclonal antibodies against the $70\ \text{kDa}$ subunit (Abcam) and core 2 subunit (Invitrogen), respectively.

Measurement of mitochondrial superoxide (O_2^-) production

Mitochondrial superoxide production was measured by dehydroethidium (DHE) (Molecular Probes), as described previously (21). Isolated mitochondria were incubated with $200\ \text{mM}$ mannitol, $70\ \text{mM}$ sucrose, $2\ \text{mM}$ HEPES pH 7.4, $0.5\ \text{mM}$ EGTA and 0.1% BSA. Reagents were added in the following order: $1\ \text{mM}$ glutamate, $1\ \text{mM}$ malate, $1\ \mu\text{M}$ DHE, $0.25\ \text{mM}$ ADP and $5\ \text{mM}$ KH_2PO_4 . Fluorescence was measured by Cytofluor 4000 (Applied biosystems) at excitation/emission = $530/620\ \text{nm}$.

Measurement of malondialdehyde in muscle

Malondialdehyde (MDA) levels were measured in muscle homogenates using an LPO-485 assay kit (BIOXYTEC), according to the manufacturer's protocol.

Western blot analysis for muscle tissue and isolated mitochondria

Proteins were extracted from quadriceps femoris muscles or mitochondria isolated from forelimb and hindlimb muscles and suspended in SDS sample buffer; $125\ \text{mM}$ Tris-HCl pH 6.8, 5% β -mercaptoethanol, 2% SDS and 10% glycerol. Extracted proteins were separated on acrylamide gels, and then transferred onto PVDF membranes (Millipore). Blocking solution of 5% skim milk was used. ImageQuant LAS 4000 Mini Biomolecular Imager (GE Healthcare) was used for evaluating bands.

Quantification of mtDNA by real-time PCR

Total DNA was isolated from triceps and quadriceps femoris and liver by proteinase K digestion and standard phenol-chloroform

extraction. Copy number of mtDNA (ND1) was quantified by real-time polymerase chain reaction (PCR) using SYBR Green PCR Kit (Qiagen) with *pcam1* as the control for the nuclear genome copy number. We used the following primers: ND1 forward primer, CCTATCACCTTGCCATCAT; ND1 reverse primer, GAGGCTGTTGCTTGTGTGAC; *pcam1* DNA forward primer, ATGGAAGCCTGCCATCATG; *pcam1* DNA reverse primer, TCCTTGTGTTTCAGCATCAC.

The amount of mtDNA relative to nuclear DNA was calculated using the following formula: $\text{mtDNA/nuclear DNA} = 2^{-(C_{\text{mtDNA}} - C_{\text{nuclearDNA}})}$ where Ct is the threshold cycle (22).

Morphometrical analysis of mitochondria

Cross-sectional EM image of extensor digitorum longus (EDL) muscle from *rmd* and littermates was analyzed by Image J software (23). Total areas of all mitochondria in 20 muscle fibers were calculated and compared with cross-sectional fiber areas. Total number of mitochondria per muscle fiber was counted.

Antibodies

Primary antibodies used were: mouse anti-4-hydroxy-2-nonenal (4-HNE) modified protein antibody (HNEJ-2, JalCA), rabbit anti-PINK1 antibody (BC100-494, Novus Biologicals), mouse anti-Parkin antibody (4211, Cell Signaling), rabbit anti-p62/SQSTM1 antibody (PWS860, Biomol), rabbit anti-LC3 antibody (NB100-2220, Novus Biologicals), mouse anti-poly-ubiquitin antibody (FK1, Biomol), rabbit anti-TOM20 antibody (FL-145, Santa Cruz), mouse anti-COX subunit 1 antibody (Invitrogen) and mouse anti-VDAC antibody (20B12, Santa Cruz). Second antibodies used were: horse radish peroxidase-labeled goat anti-mouse (Beckman Coulter) or rabbit antibodies (Cell Signaling), Alexa Fluor 488- and Alexa Fluor 568-labeled goat anti-mouse or rabbit antibodies (Invitrogen).

Statistical analysis

Data are presented as mean \pm SD. Mean differences were compared with the analysis of *t*-test using R software version 2.11.0 (<http://www.r-project.org/>).

SUPPLEMENTARY MATERIAL

Supplementary Material is available at *HMG* online.

ACKNOWLEDGEMENTS

We thank Megumu Ogawa, Kanako Goto and Junko Takei for technical assistance.

FUNDING

This study was supported partly by the Research on Psychiatric and Neurological Diseases and Mental Health of Health and Labour Sciences Research Grants; partly by the Research on Intractable Diseases of Health and Labor Sciences

Research Grants; partly by the Research Grant for Nervous and Mental Disorders (20B-12, 20B-13) from the Ministry of Health, Labour and Welfare; partly by an Intramural Research Grant (23-4, 23-5) for Neurological and Psychiatric Disorders from NCNP; partly by KAKENHI (20390250, 22791019); partly by Research on Publicly Essential Drugs and Medical Devices of Health and Labor Sciences Research Grants; partly by the Program for Promotion of Fundamental Studies in Health Sciences of the National Institute of Biomedical Innovation (NIBIO); and partly by the Grant from Japan Foundation for Neuroscience and Mental Health. G.A.C. and R.B.S. were supported in part by a National Institutes of Health Grant (AR054170 to G.A.C.).

REFERENCES

- Mitsuhashi, S., Ohkuma, A., Talim, B., Karahashi, M., Koumura, T., Aoyama, C., Kurihara, M., Quinlivan, R., Sewry, C., Mitsuhashi, H. *et al.* (2011) A congenital muscular dystrophy with mitochondrial structural abnormalities caused by defective de novo phosphatidylcholine biosynthesis. *Am. J. Hum. Genet.*, **88**, 845–851.
- Sher, R.B., Aoyama, C., Huebsch, K.A., Ji, S., Kerner, J., Yang, Y., Frankel, W.A., Hoppel, C.A., Wood, P.A., Vance, D.E. *et al.* (2006) A rostrocaudal muscular dystrophy caused by a defect in choline kinase beta, the first enzyme in phosphatidylcholine biosynthesis. *J. Biol. Chem.*, **281**, 4938–4948.
- Saraste, M. (1999) Oxidative phosphorylation at the fin de siècle. *Science*, **283**, 1488–1493.
- Spierings, D., McStay, G., Saleh, M., Bender, C., Chipuk, J., Maurer, U. and Green, D.R. (2005) Connected to death: the (unexpurgated) mitochondrial pathway of apoptosis. *Science*, **310**, 66–67.
- Wakabayashi, T. (2002) Megamitochondria formation—physiology and pathology. *J. Cell Mol. Med.*, **6**, 497–538.
- Benard, G., Bellance, N., James, D., Parrone, P., Fernandez, H. and Letellier, T. (2007) Mitochondrial bioenergetics and structural network organization. *J. Cell Sci.*, **120**, 838–848.
- Yoon, Y.S., Yoon, D.S., Lim, I.K., Yoon, S.H., Chung, H.Y., Rojo, M., Malka, F., Jou, M.J., Martinou, J.C. and Yoon, G. (2006) Formation of elongated giant mitochondria in DFO-induced cellular senescence: involvement of enhanced fusion process through modulation of Fis1. *J. Cell Physiol.*, **209**, 468–480.
- Karbowski, M., Kurono, C., Wozniak, M., Ostrowski, M., Teranishi, M., Nishizawa, Y., Usukura, J., Soji, T. and Wakabayashi, T. (1999) Free radical-induced megamitochondria formation and apoptosis. *Free Radic. Biol. Med.*, **26**, 396–409.
- Chen, H., Detmer, S.A., Ewald, A.J., Griffin, E.E., Fraser, S.E. and Chan, D.C. (2003) Mitofusins Mfn1 and Mfn2 coordinately regulate mitochondrial fusion and are essential for embryonic development. *J. Cell Biol.*, **160**, 189–200.
- Chen, H., Chomyn, A. and Chan, D.C. (2005) Disruption of fusion results in mitochondrial heterogeneity and dysfunction. *J. Biol. Chem.*, **280**, 26185–26192.
- Wu, G., Sher, R.B., Cox, G.A. and Vance, D.E. (2009) Understanding the muscular dystrophy caused by deletion of choline kinase beta in mice. *Biochim. Biophys. Acta*, **1791**, 347–356.
- Daum, G. (1985) Lipids of mitochondria. *Biochim. Biophys. Acta*, **822**, 1–42.
- Hayashi, Y.K., Matsuda, C., Ogawa, M., Goto, K., Tominaga, K., Mitsuhashi, S., Park, Y.E., Nonaka, I., Hino-Fukuyo, N., Haginoya, K. *et al.* (2009) Human PTRF mutations cause secondary deficiency of caveolins resulting in muscular dystrophy with generalized lipodystrophy. *J. Clin. Invest.*, **119**, 2623–2633.
- Bligh, E.G. and Dyer, W.J. (1959) A rapid method of total lipid extraction and purification. *Can. J. Biochem. Physiol.*, **37**, 911–917.
- Rouser, G., Fkeischer, S. and Yamamoto, A. (1970) Two dimensional thin layer chromatographic separation of polar lipids and determination of phospholipids by phosphorus analysis of spots. *Lipids*, **5**, 494–496.
- Mimaki, M., Hatakeyama, H., Ichiyama, T., Isumi, H., Furukawa, S., Akasaka, M., Kamei, A., Komaki, H., Nishino, I., Nonaka, I. *et al.* (2009)

- Different effects of novel mtDNA G3242A and G3244A base changes adjacent to a common A3243G mutation in patients with mitochondrial disorders. *Mitochondrion*, **9**, 115–122.
17. Trounce, I.A., Kim, Y.L., Jun, A.S. and Wallace, D.C. (1996) Assessment of mitochondrial oxidative phosphorylation in patient muscle biopsies, lymphoblasts, and tranmitochondrial cell lines. *Methods enzymol.*, **264**, 484–509.
 18. Vives-Bauza, C., Yang, L. and Manfredi, G. *Methods in Cell Biology. Mitochondria*, 2nd edn. Academic Press, London, UK, Vol. 80, Part 2, 7, 155–171.
 19. Tang, P.H., Miles, M.V., Miles, L., Quinlan, J., Wong, B., Wenisch, A. and Bove, K. (2004) Measurement of reduced and oxidized coenzyme Q9 and coenzyme Q10 levels in mouse tissues by HPLC with coulometric detection. *Clin. Chim. Acta*, **341**, 173–184.
 20. Wittig, I., Karas, M. and Schagger, H. (2007) High resolution clear native electrophoresis for in-gel functional assays and fluorescence studies of membrane protein complexes. *Mol. Cell Proteomics*, **6**, 1215–1225.
 21. Armstrong, J.S. and Whiteman, M. *Methods in Cell Biology. Mitochondria*, 2nd edn. Academic Press, London, UK, Vol. 80, 18, 355–377.
 22. Naini, A. and Shanske, S. *Methods in Cell Biology. Mitochondria*, 2nd edn. Academic Press, London, UK, Vol. 80, Part2, 22, 448–449.
 23. Abramoff, M.D., Magelhaes, P.J. and Ram, S.J. (2004) Image processing with Image J. *Biophotonics Int.*, **11**, 36–42.
 24. Zhang, M., Mileyskoykaya, E. and Dowhan, W. (2002) Gluing the respiratory chain together. Cardiolipin is required for supercomplex formation in the inner mitochondrial membrane. *J. Biol. Chem.*, **277**, 43553–43556.
 25. Geisler, S., Holmström, K.M., Skujat, D., Fiesel, F.C., Rothfuss, O.C., Kahle, P.J. and Springer, W. (2010) PINK1/Parkin-mediated mitophagy is dependent on VDAC1 and p62/SQSTM1. *Nat. Cell Biol.*, **12**, 119–131.
 26. Narendra, D., Tanaka, A., Suen, D.F. and Youle, R.J. (2008) Parkin is recruited selectively to impaired mitochondria and promotes their autophagy. *J. Cell Biol.*, **183**, 795–803.
 27. Lee, A.G. (2003) Lipid-protein interactions in biological membranes: a structural perspective. *Biochim. Biophys. Acta*, **1612**, 1–40.
 28. Lange, C., Nett, J.H., Trumpower, B.L. and Hunte, C. (2001) Specific roles of protein-phospholipid interactions in the yeast cytochrome bc1 complex structure. *EMBO J.*, **20**, 6591–6600.
 29. Hagopian, K., Weber, K.L., Hwee, D.T., Van Eenennaam, A.L., López-Lluch, G., Villalba, J.M., Burón, I., Navas, P., German, J.B., Watkins, S.M. *et al.* (2010) Complex I-associated hydrogen peroxide production is decreased and electron transport chain enzyme activities are altered in n-3 enriched fat-1 mice. *PLoS ONE*, **5**, e12696.
 30. Balaban, R.S., Nemoto, S. and Finkel, T. (2005) Mitochondria, oxidants, and aging. *Cell*, **120**, 483–495.
 31. St-Pierre, J., Buckingham, J.A., Roebuck, S.J. and Brand, M.D. (2002) Topology of superoxide production from different sites in the mitochondrial electron transport chain. *J. Biol. Chem.*, **277**, 44784–44790.
 32. Osaki, Y., Nishino, I., Murakami, N., Matsubayashi, K., Tsuda, K., Yokoyama, Y.I., Morita, M., Onishi, S., Goto, Y.I. and Nonaka, I. (1998) Mitochondrial abnormalities in selenium-deficient myopathy. *Muscle Nerve*, **21**, 637–639.
 33. Hill, K.E., Motley, A.K., Li, X., May, J.M. and Burk, R.F. (2001) Combined selenium and vitamin E deficiency causes fatal myopathy in guinea pigs. *J. Nutr.*, **131**, 1798–1802.
 34. Rederstorff, M., Krol, A. and Lescure, A. (2006) Understanding the importance of selenium and selenoproteins in muscle function. *Cell Mol. Life Sci.*, **63**, 52–59.
 35. Martensson, J. and Meister, A. (1989) Mitochondrial damage in muscle occurs after marked depletion of glutathione and is prevented by giving glutathione monoester. *Proc. Natl Acad. Sci. USA*, **86**, 471–475.
 36. Choksi, K.B., Boylston, W.H., Rabek, J.P., Widger, W.R. and Papaconstantinou, J. (2004) Oxidatively damaged proteins of heart mitochondrial electron transport complexes. *Biochim. Biophys. Acta*, **1688**, 95–101.
 37. Kim, I., Rodriguez-Enriquez, S. and Lemasters, J. (2007) Selective degradation of mitochondria by mitophagy. *Arch. Biochem. Biophys.*, **462**, 245–253.
 38. Tatsuta, T. and Langer, T. (2008) Quality control of mitochondria: protection against neurodegeneration and ageing. *EMBO J.*, **27**, 306–314.
 39. Ding, W.X., Ni, H.M., Li, M., Liao, Y., Chen, X., Stolz, D.B., Dorn, G.W. 2nd. and Yin, X.M. (2010) Nix is critical to two distinct phases of mitophagy, reactive oxygen species-mediated autophagy induction and Parkin-ubiquitin-p62-mediated mitochondrial priming. *J. Biol. Chem.*, **285**, 27879–27890.
 40. Moraes, C.T., Shanske, S., Tritschler, H.J., Aprille, J.R., Andreetta, F., Bonilla, E., Schon, E.A. and DiMauro, S. (1991) mtDNA depletion with variable tissue expression: a novel genetic abnormality in mitochondrial diseases. *Am. J. Hum. Genet.*, **48**, 492–501.
 41. Kim, I. and Lemasters, J.J. (2011) Mitochondrial degradation by autophagy (mitophagy) in GFP-LC3 transgenic hepatocytes during nutrient deprivation. *Am. J. Physiol. Cell Physiol.*, **300**, C308–C317.

Proteolytic processing regulates pathological accumulation in dentatorubral-pallidolusian atrophy

Yasuyo Suzuki¹, Kimiko Nakayama¹, Naohiro Hashimoto² and Ikuru Yazawa¹

¹ Laboratory of Research Resources, Research Institute for Longevity Sciences, National Center for Geriatrics and Gerontology, Aichi, Japan

² Department of Regenerative Medicine, Research Institute for Longevity Sciences, National Center for Geriatrics and Gerontology, Aichi, Japan

Keywords

atrophin-1; dentatorubral-pallidolusian atrophy; DRPLA; DRPLA protein; neurodegeneration; polyglutamine

Correspondence

I. Yazawa, Laboratory of Research Resources, Research Institute for Longevity Sciences, National Center for Geriatrics and Gerontology, 35 Gengo, Morioka-cho, Obu-shi, Aichi 474-7511, Japan
Fax: +81 562 46 8319
Tel: +81 562 46 2311
E-mail: yazawa@nils.go.jp

(Received 27 July 2010, revised 9 September 2010, accepted 23 September 2010)

doi:10.1111/j.1742-4658.2010.07893.x

Dentatorubral-pallidolusian atrophy is caused by polyglutamine (polyQ) expansion in atrophin-1 (ATN1). Recent studies have shown that nuclear accumulation of ATN1 and cleaved fragments with expanded polyQ is the pathological process underlying neurodegeneration in dentatorubral-pallidolusian atrophy. However, the mechanism underlying the proteolytic processing of ATN1 remains unclear. In the present study, we examined the proteolytic processing of ATN1 aiming to understand the mechanisms of ATN1 accumulation with polyQ expansion. Using COS-7 and Neuro2a cells that express the *ATN1* gene, in which ATN1 was accumulated by increasing the number of polyQs, we identified a novel C-terminal fragment containing a polyQ tract. The mutant C-terminal fragment with expanded polyQ selectively accumulated in the cells, and this was also demonstrated in the brain tissues of patients with dentatorubral-pallidolusian atrophy. Immunocytochemical and biochemical studies revealed that full-length ATN1 and C-terminal fragments displayed individual localization. The mutant C-terminal fragment was preferentially found in the cytoplasmic membrane/organelle and insoluble fractions. Accordingly, it is assumed that the proteolytic processing of ATN1 regulates the localization of C-terminal fragments. Accumulation of the C-terminal fragment was enhanced by inhibition of caspases in the cytoplasm of COS-7 cells. Collectively, these results suggest that the C-terminal fragment plays a principal role in the pathological accumulation of ATN1 in dentatorubral-pallidolusian atrophy.

Introduction

The polyglutamine (polyQ) diseases are a group of hereditary neurodegenerative disorders that include Huntington's disease (HD), dentatorubral-pallidolusian atrophy (DRPLA), spinal and bulbar muscular atrophy, and several forms of spinocerebellar ataxia [1–3]. These diseases are caused by expansion of CAG trinucleotide repeats that encode a polyQ tract in the

responsible genes. Aside from the CAG trinucleotide repeat, the genes responsible for the various polyQ diseases have no homology to one other. Therefore, speculation concerning the pathogenesis has been focused on the expanded polyQ itself, which appears to cause the gene products to undergo a conformational change that makes them aggregate in neurones [4]. This

Abbreviations

ALLN, *N*-acetyl-Leu-Leu-norleucinal; ATN1, atrophin-1; DRPLA, dentatorubral-pallidolusian atrophy; GFP, green fluorescent protein; HD, Huntington's disease; HRP, horseradish peroxidase; NLS, nuclear localizing signal; polyQ, polyglutamine; TPEN, *N,N,N',N'*-tetrakis(2-pyridylmethyl)ethylenediamine; TUNEL, terminal deoxynucleotidyl transferase-mediated dUTP nick end labelling; Z-VAD-FMK, benzyloxycarbonyl-Val-Ala-Asp(OMe)-fluoromethyl ketone.